J. Fluid Mech. (1998), *vol.* 373, *pp.* 313–348. Printed in the United Kingdom

Turbulent combined oscillatory flow and current in a pipe

By C. R. LODAHL, B. M. SUMER AND J. FREDSØE

Technical University of Denmark, Department of Hydrodynamics and Water Resources (ISVA), 2800 Lyngby, Denmark

(Received 24 November 1997 and in revised form 18 May 1998)

This work concerns the combined oscillatory flow and current in a circular, smooth pipe. The study comprises wall shear stress measurements, and laser-Doppler-anemometer velocity and turbulence measurements. Three kinds of pipes were used, with diameters $D = 19$ cm, 9 cm, and 1.1 cm, enabling the influence of the parameter R/δ to be studied in the investigation (R/δ ranging from about 3 to 53), where R is the radius of the pipe, and δ is the Stokes layer thickness. The ranges of the two other parameters of the combined flow processes, namely the current Reynolds number, Re_c, and the oscillatory-flow boundary-layer (i.e. the wave–boundary layer) Reynolds number, Re_w, are: $Re_c = 0$–1.6×10^5, and $Re_w = 0$–7×10^6. The transition to turbulence in the combined flow case occurs at a current Reynolds number larger than the conventional value, *ca.* 2×10^3, depending on Re_w, and R/δ. A turbulent current can be laminarized by superimposing an oscillatory flow. The overall average value of the wall shear stress (the mean wall shear stress) may retain its steady-current value, it may decrease, or it may increase, depending on the flow regime. The increase (which can be as much as a factor of 4) occurs when the combined flow is in the wave-dominated regime, while the oscillatory-flow component of the flow is in the turbulent regime. The component of the wall shear stress oscillating around the mean wall shear stress can also increase with respect to its oscillatory-flow-alone value. For this to occur, the originally laminar oscillatory boundary layer needs to become a fully developed turbulent boundary layer, when a turbulent current is superimposed. This increase can be as much as $O(3$–$4)$. The velocity profiles across the cross-section of the pipe change near the wall when an oscillatory flow is superimposed on a current, in agreement with the results of the wall shear stress measurements. The period-averaged turbulence profiles across the cross-section of the pipe behave differently for different flow regimes. When the two components of the flow are equally significant, the turbulence profile appears to be different from those corresponding to the fundamental cases; the level of turbulence increases (only slightly) with respect to those experienced in the fundamental cases.

1. Introduction

Waves in a coastal environment usually co-exist with currents. The waves and currents interact through a number of mechanisms such as modification of the wave kinematics by the current, modification of the current (over the entire flow depth) by the presence of the waves, and the interaction of the wave and current boundary layers. The present study concerns the wave–current interaction within the bottom boundary layer.

The wave–current boundary layer interaction has been the subject of a great many

investigations in the last decade or so; Bakker & van Doorn (1978), Kemp & Simons (1982, 1983), Asano, Nakagawa & Iwagaki (1986), Myrhaug, Reed & Fyfe (1987), Simons *et al.* (1988), Sleath (1990), Simons, Grass & Mansour-Tehrani (1992), Arnskov, Fredsøe & Sumer (1993), and Simons *et al.* (1994) on the experimental side; Bijker (1967), Grant & Madsen (1979), Fredsøe (1984), van Kesteren & Bakker (1984), Christoffersen & Jonsson (1985), Justesen (1988), Davies, Soulsby & King (1988), Myrhaug & Slaattelid (1990), Huynh-Thanh & Temperville (1991) and Sleath (1991), among others, on the theoretical side. Field work has also been carried out, notably by Grant *et al.* (1983), Huntley & Hazen (1988), Myrhaug & Slaattelid (1989), and Soulsby & Humphery (1990). A recent major review on the subject has been published by Soulsby *et al.* (1993).

The previously mentioned research has shown that a wave field superimposed on a current may change the mean and turbulence properties of the bottom boundary layer significantly, therefore influencing the sediment transport to a large degree. The aforementioned changes in the flow may include the following processes. (i) The mean bed shear stress may increase, or remain constant, or even decrease (as will be demonstrated in the present study) with respect to its steady-current value. (ii) Likewise, the maximum bed shear stress may increase, or it may retain its steady-current value when the waves are introduced. (iii) Furthermore, the turbulence in the bed shear stress may be suppressed, or it may even completely disappear when waves are superimposed on a current (as first observed by Gilbrech & Combs 1963 and Sarpkaya 1966). Although the previously mentioned research has thrown considerable light on the wave–current boundary layer interaction, comparatively little is known about the mechanics of the complex flow processes in this interaction mechanism. No clear, comprehensive understanding of these processes is yet available.

The purpose of the present investigation is to study these flow processes in a 'clean' wave–current flow environment where the oscillating component of the flow (induced by real waves) is simulated by an oscillatory flow (in an oscillatory water tunnel, as described in §2), thereby eliminating the additional effects such as wave nonlinearity and wave asymmetry, plus more importantly enabling the 'full scale' wave-induced velocities (hence, the fully developed turbulent wave-boundary layer conditions) to be produced under laboratory conditions, a feature which could not be fully achieved in the previous research. Furthermore, a circular pipe has been adopted in the present study in favour of a rectangular cross-section tunnel, to experiment with a truly two-dimensional wave–current flow, without any kind of secondary currents, which are unavoidable in a rectangular cross-section flow environment.

There exists quite a substantial literature on 'pulsating Poiseuille flows' in circular pipes: Gilbrech & Combs (1963), Sarpkaya (1966), Tromans (1978), Ramaprian & Tu (1980, 1983), Tu & Ramaprian (1983), Shemer, Wygnanski & Kit (1985), Mao & Hanratty (1986, 1994), Stettler & Hussain (1986), Finnicum & Hanratty (1988). Tardu, Binder & Blackwelder (1994), on the other hand, studied the pulsating Poiseuille flow in a channel. However, the common features of these studies are that (i) the combined oscillatory flow and current is always in the current-dominated flow regime, and (ii) the oscillatory component of the flow is in the laminar- or transitional-flow regime. Therefore, various characteristics of the combined flow associated with the wave-dominated, fully developed turbulent wave-boundary-layer flows (such as the increase in the mean wall shear stress, and the increase in the maximum wall shear stress, as will be demonstrated in the present paper) could not be captured.

The present study covers practically the entire range of wave–current flows, namely from the current-dominated-flow regime to the wave-dominated-flow regime, and from

the laminar-wave-boundary-layer flow regime to the fully developed-turbulent-wave-boundary-layer flow regime. The mechanisms governing the various flow processes in the bottom boundary layer are also discussed.

2. Experimental set-up

The experiments were carried out in a U-shaped oscillatory water tunnel, 10 m in length (plus a 2.2 m long contraction section at the two ends), 0.39 m in width and 0.29 m in height. The tunnel is the same as that described in Jensen, Sumer & Fredsøe (1989). The top and the side walls of the tunnel are made of smooth transparent Perspex plates.

The flow environment of the present study was a circular pipe, as mentioned in the previous section. The pipe was placed in the tunnel (figures 1 *a* and 1 *c*), and rigidly fixed to it. Three kinds of pipes were used in the experiments, with diameters $D = 19$ cm, 9 cm, and 1.1 cm. Different pipe diameters make it possible to vary the parameter R/δ (one of the parameters of the study) significantly, as will be seen later in the paper. Here, R is the radius of the pipe, and δ is the Stokes layer thickness defined by

$$\delta = (2\nu/\omega)^{1/2}, \tag{1}$$

in which $\omega = 2\pi/T$ is the angular frequency of the oscillatory component of the combined flow, T is the period, and ν is the kinematic viscosity. These transparent Perspex pipes had trumpet-mouth inlets at both ends. The pipes' surface was smooth. No water flow was allowed in the space between the pipe and the tunnel. The 19 cm pipe was 10 m long, extending along the entire length (10 m) of the working section of the tunnel, while the 9 cm pipe was 7.5 m long, and the 1.1 cm pipe was 5 m long. The selection of the lengths of the latter two pipes are simply for convenience.

The movement of the pipe walls was checked under varying pressure, and was found to be virtually nil.

The current in the tunnel was provided by a constant head tank, the head being 6 m with respect to the mean water level in the risers of the tunnel. The desired flow rate was obtained by simultaneous adjustments of the inlet and the outlet valves of the tunnel (figure 1 *c*). The flow rate itself was measured by a magnetic flow meter installed on the supply pipe (figure 1 *c*) before the pipe enters the tunnel.

The oscillatory flow in the tunnel is driven by an electronically controlled pneumatic system (figure 1 *c*) in exactly the same fashion as in Jensen *et al.*'s (1989) study.

The procedure adopted in the case of a combined flow is described in detail in §2.3. The measured velocity profiles across the pipe cross-section revealed that the flow rate in the combined flow case was maintained the same as in the current-alone situation (within less than 1 %).

The centreline velocity, and, in some cases, the water level in the open riser of the tunnel were used as the reference signal.

Two kinds of measurements were made: the wall shear stress measurements, and the velocity profile measurements. All the measurements were made in the middle section of the tunnel (5 m downstream from the junction between the contraction section and the working section).

2.1. *The wall shear stress measurements*

The wall shear stress was measured with a Dantec 9055 R 0461 hot-film probe. The probe was mounted flush to the wall of the pipe (figure 1 *a*). The size of the thermal element in the probe was 0.75 mm, meaning that the wall shear-stress signal is averaged

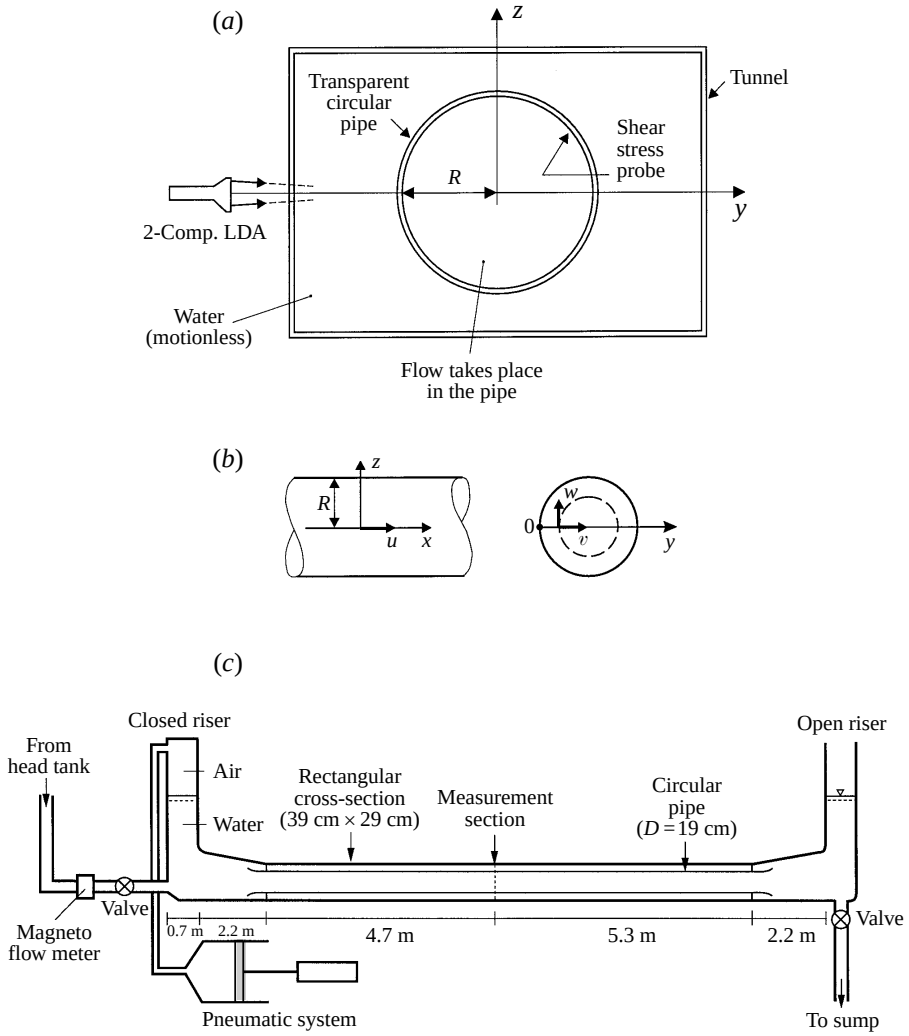

FIGURE 1. (*a*) Cross-section of the experimental tunnel and the pipe. (*b*) Definition sketch. (*c*) Schematic of the set up.

out over a distance in the transverse direction of $lU_f/\nu = O(7.5)$ for a wall shear-stress velocity of $U_f = O(1\ \mathrm{cm\ s^{-1}})$, and $O(75)$ for a wall shear stress velocity of $U_f = O(10\ \mathrm{cm\ s^{-1}})$. Details of the measurement technique and the accuracy of the instrument are given in Sumer *et al.* (1993).

The calibration of the probe at small wall shear stresses was made *in situ*, determining the calibration coefficients A and B in the calibration relation

$$\tau_0^{1/3} = AE^2 + B \tag{2}$$

using the relationship between the centreline velocity and the wall shear stress in the case of a laminar oscillatory flow in the pipe. Here E is the voltage drop. For turbulent flows, (2) holds provided that τ_0 is the instantaneous value of the wall shear stress, and E the corresponding instantaneous voltage drop (Hanratty & Campbell 1983). It may

be noted that the calibration curve at higher shear stresses obtained in our earlier work with a three-sided calibration channel (1 mm in depth and 30 mm in width, placed over the probe in the case of a plane boundary) confirmed this.

In the case of the combined current and oscillatory flow, the velocity of the fluid just above the shear stress probe was measured with a two-component laser-Doppler-anemometer (LDA), to detect the direction of the wall shear stress when it is not straightforward from the wall-shear-stress measurement itself (e.g. in the case of the combined flow where the current velocity and the maximum value of the oscillatory flow velocity are quite close to each other).

The wall shear stress measurements were not made in the 1.1 cm diameter pipe, because the size of the housing of the hot-film probe (2 mm in diameter) was too big with respect to the rather small size of the pipe.

2.2. *The velocity profile measurements*

The velocity profile measurements (including the turbulence profiles) were made in the 19 cm diameter pipe, using a two-component LDA system – a fibre optic LDA system consisting of a 100 mW argon laser, two Dantec 55N10 frequency shifters and two Dantec 55N20 frequency trackers. The measured velocity components are: x- (the streamwise) and z- (the tangential) velocity components, u and w, respectively (figure 1*b*). The LDA probe was traversed along the y-axis over the entire radius of the pipe (figure 1*a*) for these measurements. The measurement of the velocity component normal to the wall (the v-component) was not straightforward; the u- and w-measurements were performed by shooting the laser in the plane passing through the centre of the pipe so that the laser beam reached the pipe at a right angle, whereas with any other shooting angle, some deflection of the laser beam might occur, and this creates a problem in determining the location of the actual measurement point in a closed environment like the present one, particularly near the wall. For this reason, the measurement of the velocity component normal to the wall was abandoned in the present study.

A one-component LDA system, a 15 mW He–Ne laser equipped with a Dantec 55N10 frequency shifter and a Dantec 55N20 frequency tracker, was used to monitor the centreline velocity in the pipe.

Both LDA system were used in forward scatter mode. The dimensions of the measuring volume were $(d_x \times d_y \times d_z) = 0.15\ \text{mm} \times 2.5\ \text{mm} \times 0.15\ \text{mm}$ for the two-component LDA, and $(d_x \times d_y \times d_z) = 0.6\ \text{mm} \times 12.0\ \text{mm} \times 0.6\ \text{mm}$ for the one-component LDA.

The measurements were made with a sampling interval of 24 ms, corresponding to 416 samples per cycle. In the turbulent flow regime, at least 50 cycles were sampled in each test. In the laminar oscillatory flow case, typically 5 cycles were sampled. The recorded time series in this latter case revealed that the successive periods of the motion were virtually the same.

In the case of a steady current, mean values were obtained through time-averaging, the sampling time for which was about 5 minutes.

In the case of an oscillatory flow, and also in the case of a combined oscillatory flow and current, mean values were calculated through ensemble averaging, e.g.

$$\tilde{\tau}_0(\omega t) = \frac{1}{N}\sum_{j=1}^{N} \tau_0[\omega(t+(j-1)\,T)], \tag{3}$$

in which $\tilde{\tau}_0$ is the ensemble-mean wall shear stress, ω is the angular frequency of the oscillatory flow, t is the time, and N is the total number of cycles sampled.

2.3. *Experimental procedure*

The experimental procedure adopted in a typical experiment to measure the wall shear stress in combined flows was as follows: (i) First the wall shear-stress probe was calibrated. (ii) Subsequently, the desired current was established in the pipe, and the 'current alone' measurements (the centre line velocity and shear stress measurements) were made. (iii) Then the first oscillatory motion was superimposed, and the corresponding wall shear stress measurement was made. Here, the desired oscillatory flow was achieved in the combined flow by driving the piston of the pneumatic system at the desired amplitude. Furthermore, the flow rate was monitored constantly by the previously mentioned magnetic flow meter, to check if it was maintained constant. (iv) The previous step was repeated for further increases in the velocity of the oscillatory flow. (v) Upon the completion of the test program corresponding to that particular current, the wall shear stress probe was calibrated again. If there was a change in the calibration, the entire data set was rejected. (This was the case in a few tests.)

In the case of the velocity profile measurements, the same procedure was adopted.

3. Test conditions

3.1. *Fundamental case 1. Current-alone tests*

Table 1 summarizes the test conditions for the measurements in the current-alone tests. In the table, U_{cl} is the centreline velocity, V is the cross-sectional mean velocity (obtained from the measured velocity profiles), τ_0 is the wall shear stress, ρ is the fluid density, and Re_c is the Reynolds number defined by

$$Re_c = DV/\nu. \tag{4}$$

3.2. *Fundamental case 2. Oscillatory-flow-alone tests*

Table 2 summarizes the test conditions for the measurements in the oscillatory-flow-alone case. In the table, U_m is the maximum value of the sinusoidal oscillatory flow velocity at the centreline of the pipe, i.e.

$$U = U_m \sin(\omega t), \tag{5}$$

a is the amplitude of the oscillatory flow at the same location (calculated as $a = U_m T/(2\pi)$), and Re_w is the Reynolds number of the oscillatory boundary-layer flow, defined by

$$Re_w = aU_m/\nu. \tag{6}$$

Note that U_m values quoted in the table are directly measured values.

3.3. *Combined oscillatory flow and current tests*

The test conditions corresponding to these tests are summarized in table 3. The procedure followed in these tests has been described in §2.3. The V and U_m values quoted in the table are those values corresponding to the steady-current and the oscillatory-flow components, respectively.

As seen from the table, a total of 96 combinations of current and oscillatory flow was achieved in the 19 cm diameter pipe. This figure was 72 for the 9 cm diameter pipe and 24 for the 1.1 cm diameter pipe.

D (cm)	U_{cl} (m s^{-1})	V (m s^{-1})	Re_c	Measured quantities	Total number of tests
19	0.023–0.94	0.012–0.84	2.2×10^3–1.6×10^5	$U_{cl}, u(y), \tau_0$	7
19	0.17	0.14	2.7×10^4	$U_{cl}, \tau_0, u(y), w(y)$	1
19	0.94	0.84	1.6×10^5	$U_{cl}, \tau_0, u(y), w(y)$	1
9.0	0.044–2.15	0.222–1.77	2.0×10^3–5.5×10^5	$U_{cl}, \tau_0, u(y), w(y)$	6
1.1	0.43; 0.46	0.22; 0.23	2.4×10^3; 2.5×10^3	U_{cl}	2

TABLE 1. Test conditions for the fundamental case: current alone

D (cm)	T (s)	U_m (m s^{-1})	a (m)	Re_w	R/δ	Measured quantities	Total number of tests
19	10	0.01–1.17	0.016–1.86	2×10^2–2.2×10^6	53	U_{cl}, τ_0	47
19	10	0.62	0.98	6×10^5	53	$U_{cl}, u(y), \tau_0$	1
19	10	1.14	1.81	2.1×10^6	53	$U_{cl}, u(y), \tau_0$	1
9.0	10	0.038–2.5	0.06–3.98	2.3×10^3–9.9×10^6	25	U_{cl}, τ_0	18
1.1	5.3	0.67	0.56	3.8×10^5	4.2	U_{cl}	1
1.1	10	1.18	1.88	2.2×10^6	3.1	U_{cl}	1

TABLE 2. Test conditions for the fundamental case: oscillatory-flow alone

4. Laminar-to-turbulent transition

4.1. *Oscillatory flow alone*

The transition to turbulence is governed by two non-dimensional quantities in this case, namely the oscillatory-flow Reynolds number, and the radius-to-Stokes'-layer-thickness ratio:

$$Re_w \quad \text{and} \quad R/\delta. \tag{7}$$

Figure 2 illustrates the time series of $|\tau_0|$, the absolute value of the wall shear stress, for the case where $Re_w = 1.8\times10^5$ and $R/\delta = 53$. As seen, turbulence first emerges just prior to the wall shear stress reversal (the spikes prior to the wall shear stress reversals are marked by arrows), similar to the results of Hino, Sawamoto & Takasu (1976) and Jensen *et al.* (1989). Kemp & Simons (1982) also noted high turbulence in the decelerating phase. This is because the adverse pressure gradient becomes relatively large, and the near-wall velocities become relatively small at these phase values, presumably leading to a favourable environment for the initiation of turbulence. Some researchers like Foster, Holman & Beach (1994), and Foster (1996) have suggested that the turbulence here is caused by a shear instability of the velocity profile which, at this phase, has an inflection point.

Figure 3 depicts the transition-to-turbulence data on the plane of the Reynolds number, Re_w, and the radius-to-Stokes'-layer-thickness ratio, R/δ. In the figure, Tromans' (1978) result obtained from the linear stability analysis is also plotted. Note that the transition to turbulence in the present tests was judged to occur when there was any sign of imperfection in the wall shear stress signal, certainly different from the typical smooth, laminar-flow signal. The latter normally emerged in the deceleration stage in the form of spikes, as described in the preceding paragraphs, and also in Jensen *et al.* (1989).

D (cm)	V (m s^{-1})	Re_c	T (s)	U_m (m s^{-1})	Re_w	R/δ	V/U_m	Measured quantities	Total number of tests
19	0.008–0.84	1.5×10^3–1.6×10^5	10	0.01–1.06* and 0.04–1.17**	2×10^2–1.8×10^6* and 2×10^3–2.2×10^6**	53	0.03–2.8* and 0.7–24.3**	U_{cl}, τ_0	90
19	0.14	2.7×10^4	10	0.64–2.04	7×10^5–7×10^6	53	0.07–0.22	U_{cl}, τ_0, u, w	3
19	0.84	1.6×10^5	10	0.64–2.04	7×10^5–7×10^6	53	0.41–1.3	U_{cl}, τ_0, u, w	3
9.0	0.032–1.77	2.9×10^3–5.5×10^4	10	0.04–2.41* and 0.16–2.43**	2.5×10^3–9.2×10^6* and 4.2×10^4–9.4×10^6**	25	0.03–1.8* and 3.75–0.25**	U_{cl}, τ_0	72
1.1	0.13–0.34	1.4–3.7×10^3	5.3	0.19–0.67	3×10^4–3.8×10^5	4.2	0.2–1.3	U_{cl}	13
1.1	0.09–0.31	1–3.5×10^3	10	0.21–1.2	7×10^4–2.3×10^6	3.1	0.08–1.4	U_{cl}	11

TABLE 3. Test conditions for the combined oscillatory flow and current tests. Single asterisk corresponds to $Re_c = 6\times10^3$, and double asterisk corresponds to $Re_c = 1.6\times10^5$ for $D = 19$ cm pipe, and to $Re_c = 5.5\times10^4$ for $D = 9$ cm pipe

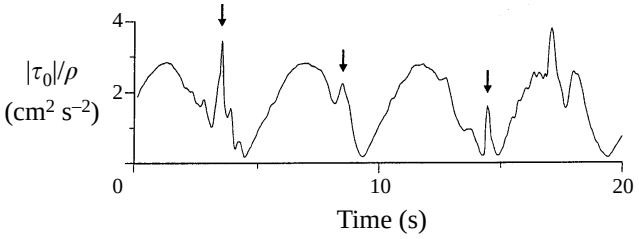

FIGURE 2. Time series of the wall shear stress in oscillatory flow alone. $R/\delta = 53$, $Re_w = 1.8 \times 10^5$.

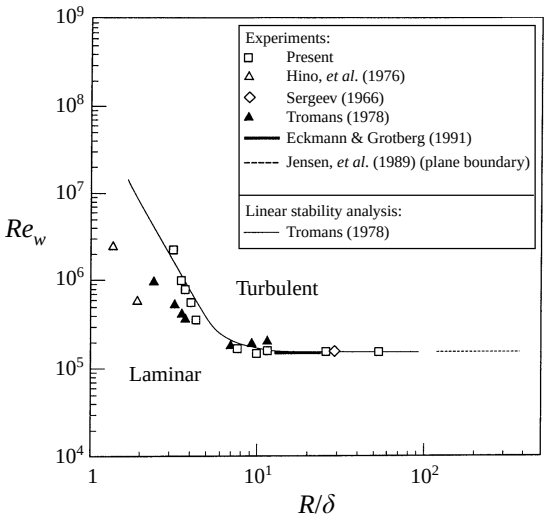

FIGURE 3. Transition to turbulence in oscillatory flow alone.

From figure 3, the present data and the data from other researchers except Hino *et al.* (1976) appear to be in agreement. It is also seen that the present data are in very good agreement with the Tromans stability curve. There is, however, a marked discrepancy between the data of Hino *et al.* and those of others. No clear explanation has been found for this.

Secondly, from figure 3, the critical value of Re_w approaches the asymptotic value $Re_w = 1.5 \times 10^5$, as $R/\delta \to \infty$, i.e. the critical value of the Reynolds number for transition known from the plane-wall oscillatory flow research (see e.g. Jensen *et al.* 1989), as expected.

Thirdly, the critical value of Re_w begins to increase, as R/δ decreases ($R/\delta \lesssim 10$). This behaviour is, in fact, expected: as $R/\delta \to 0$, the flow will behave like a steady pipe flow, meaning that the governing parameters, namely Re_w and R/δ, should reduce to $U_m D/\nu$ (or, alternatively to VD/ν, where $V = \frac{1}{2}U_m$), the parameter which governs the steady pipe flow. This is possible only for one combination of Re_w and R/δ, namely $Re_w(R/\delta)^2$, as seen from

$$RE_w\left(\frac{R}{\delta}\right)^2 = \frac{1}{8}\left(\frac{U_m D}{\nu}\right)^2. \tag{8}$$

The transition to turbulence in this asymptotic case occurs when $U_m D/\nu$ (or, alternatively VD/ν) reaches a certain value. Hence in this asymptotic case, the transition occurs for a critical value of $Re_w(R/\delta)^2$. This clearly shows that the critical

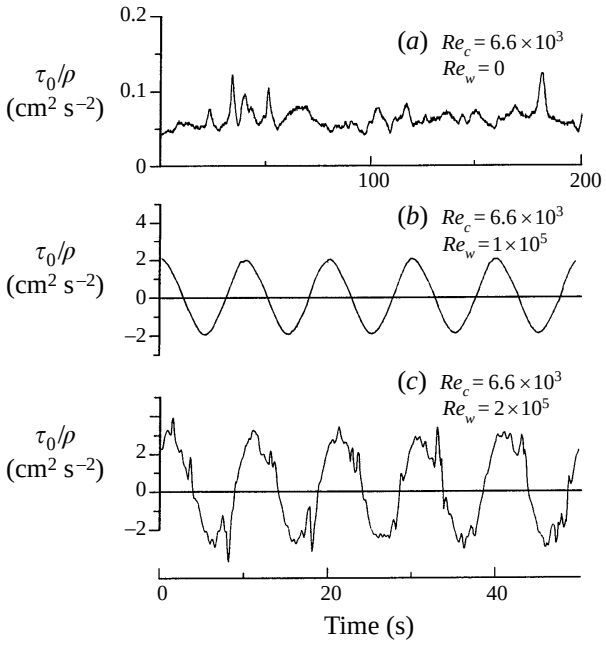

FIGURE 4. Time series of the wall shear stress. $R/\delta = 53$.

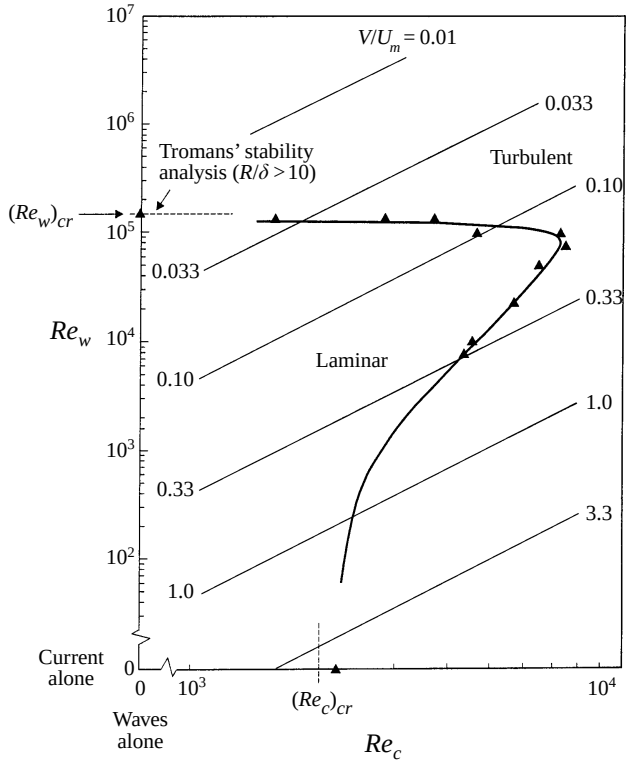

FIGURE 5. Transition to turbulence in combined flow. $R/\delta = 53$.

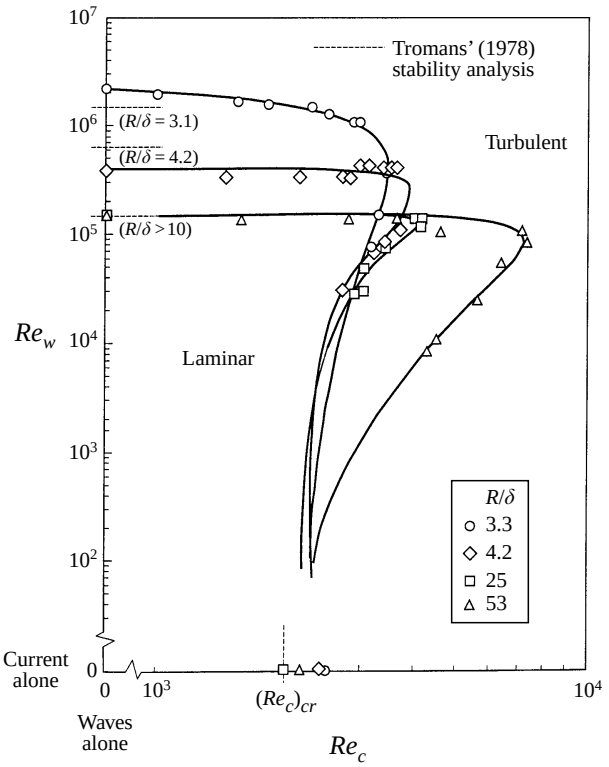

FIGURE 6. Transition to turbulence in combined flow for four different values of R/δ.

value of Re_w should increase with decreasing R/δ, as $R/\delta \to 0$. (When $V = \frac{1}{2}U_m$ is inserted in (8), and the critical value of VD/ν is taken as 2×10^3, the critical value of $Re_w(R/\delta)^2$ for transition is found to be 2×10^6.)

4.2. *Combined oscillatory flow and current*

In the case of combined flows, in addition to the non-dimensional quantities given in (7), the current Reynolds number Re_c should also be involved. Hence, the transition to turbulence is governed by the following three non-dimensional quantities:

$$Re_w, R/\delta \quad \text{and} \quad Re_c. \tag{9}$$

Figure 4 presents the time series of the wall shear stress for three different combinations of the oscillatory flow and the current for the 19 cm diameter pipe ($R/\delta = 53$). In figure 4(*a*) the oscillatory component in zero and the current has $Re_c = 6.6 \times 10^3$; the flow is in the turbulent regime. In figure 4(*b*) the oscillatory flow is introduced corresponding to an oscillatory-flow Reynolds number of $Re_w = 10^5$, while the current component (hence Re_c) is maintained the same as before. In figure 4(*c*) the oscillatory flow velocity is increased by a factor of 2 ($Re_w = 2 \times 10^5$), while still keeping the current Re_c the same. As seen clearly from figure 4(*b*), with the introduction of the oscillatory flow, the flow is laminarized. However, when Re_w is increased by a factor of 2 in figure 4(*c*) the flow becomes turbulent again; the transition to turbulence occurs in the deceleration stage just prior to the reversal of the wall shear stress, in much the same way as in figure 2.

Figure 5 presents the transition data, on the (Re_w, Re_c)-plane, obtained for the 19 cm

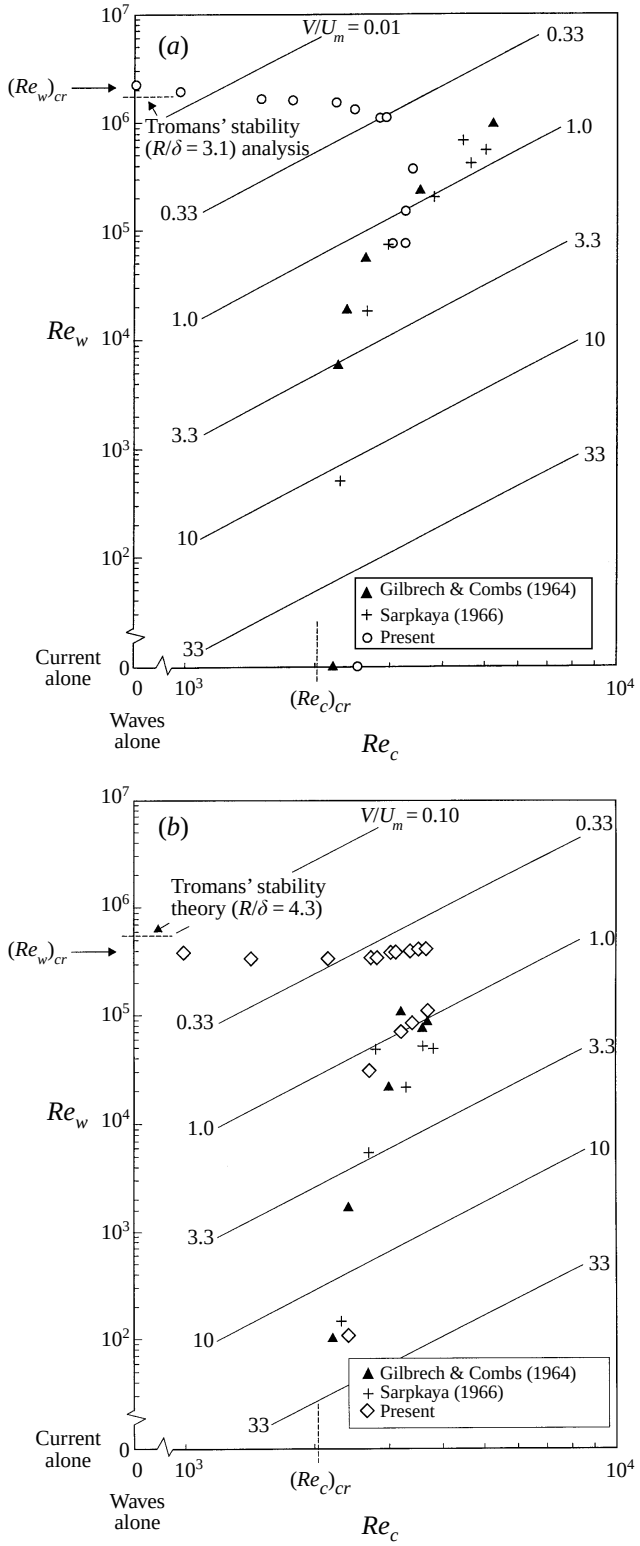

FIGURE 7. Transition to turbulence in combined flow. Comparison with the results of other researchers. (*a*) $R/\delta = 3.1$, (*b*) $R/\delta = 4.2$.

diameter pipe ($R/\delta = 53$). Figure 5 also contains the contour plot of V/U_m. We shall return to this later in the section.

First, the data in figure 5 indicate that (i) the critical value of Re_c approaches $(Re_c)_{cr} \approx 2 \times 10^3$, as $Re_w \to 0$ (the value known from the steady pipe flow research, Schlichting 1979, p. 451), and (ii) the critical value of Re_w approaches $(Re_w)_{cr} = 1.5 \times 10^5$, as $Re_c \to 0$ (the value obtained from the oscillatory-flow-alone tests and from the linear stability analysis, figure 3).

Secondly, the transition to turbulence is delayed by superimposing an oscillatory flow on the current; while the transition occurs at $Re_c \approx 2 \times 10^3$ in the case of the pure current, it occurs only after Re_c reaches a value of about 7.5×10^3 in the case of the combined flow with $Re_w = 8 \times 10^4$, a factor of 3.5 increase in the critical value of the Reynolds number Re_c.

Thirdly, the figure indicates that a turbulent current flow can be laminarized by introducing an oscillatory flow (cf. figure 4*b*). It shows that the Re_w range where the flow is laminarized varies with the current Reynolds number Re_c: for the data given in figure 5, this range extends from $Re_w \approx 10^3$ to $Re_w \approx 1.5 \times 10^5$ for $Re_c = 3 \times 10^3$, and from $Re_w \approx 3 \times 10^4$ to $Re_w \approx 1.5 \times 10^5$ for $Re_c = 6 \times 10^3$. (This process, termed the re-laminarization, has been recognized by earlier researchers such as Gilbrech & Combs 1963, Sarpkaya 1966, and Ramaprian & Tu 1980).

This paragraph will address the issue of the re-laminarization. Figure 5 depicts the V/U_m = constant lines. These lines were obtained from

$$\frac{V}{U_m} = \frac{1}{2\sqrt{2}} \frac{Re_c}{(R/\delta)\, Re_w^{1/2}}. \tag{10}$$

Small values of V/U_m such as $V/U_m = O(0.1)$ mean that the combined flow will be dominated by its oscillatory-flow component (hereafter called the 'wave-dominated flow'). A close inspection of figure 5 together with figure 3 apparently indicates that, in the wave-dominated case, the flow regime is actually determined by the regime of the oscillatory-flow component itself: if the oscillatory component is in the laminar regime, then the combined flow will also be in the laminar regime, and vice versa, regardless of the regime of the current component of the combined flow. So, for the re-laminarization of the flow to occur, first and foremost the velocity ratio V/U_m should be sufficiently small so that the flow becomes wave dominated, and secondly the Reynolds number of the oscillatory component of the flow, Re_w, should be sufficiently small so that the oscillatory component of the flow is in the laminar flow regime (figure 3). Other tests conducted in the present study with different values of R/δ all indicated the same behaviour (see figures 6 and 7).

It may be argued that the relaminarization occurs because the current turbulence is suppressed by the waves of vorticity of alternating signs that rise from the surface. However, in view of the results described in the preceding paragraphs, this argument may not be always true. For example, the present results imply that a large-Reynolds-number steady-current flow may not be laminarized by superimposing an oscillatory flow, simply because that may require a large-Reynolds-number oscillatory flow for the combined flow to be a wave-dominated flow (one of the requirements of the relaminarization), and obviously this kind of large Reynolds-number oscillatory flow will most likely be in the transition/turbulent regime, meaning that the re-laminarization may never be achieved.

It is interesting to note that the way in which the transition to turbulence occurs in the re-laminarized flow (figure 4*c*) is much the same as in the case of the oscillatory flow

alone (cf. figure 2; the occurrence of spikes in the deceleration stage just prior to the reversal of the wall shear stress). This suggests that basically the transition to turbulence occurs due to the transition in the oscillatory component of the flow in this case.

Figure 6 presents the transition-to-turbulence data for the other R/δ values of the present study. Tromans' (1978) results from the linear stability analysis (figure 3) have also been plotted in the diagram as the asymptotic lines for the limit $Re_c \to 0$ (the oscillatory-flow-alone case). The figure shows that the range of the current Reynolds number, Re_c, over which the re-laminarization occurs becomes narrower and narrower with decreasing R/δ (while this range is $Re_c = 2\times10^3$–7.5×10^3 for $R/\delta = 53$, it is only $Re_c = 2\times10^3$–3.5×10^3 for $R/\delta = 3.3$). This is consistent with the fact that when $R/\delta \to 0$ (the quasi-steady pipe flow), obviously no re-laminarization should occur, and hence the previously mentioned range of Re_c should shrink to zero.

Figures 7(*a*) and 7(*b*) compare the present data with those obtained by Gilbrech & Combs (1964) and Sarpkaya (1966). The agreement is quite good. As seen from the figure, the previous research covers only the current-dominated flow regime ($V/U_m \gtrsim 0.7$ in figure 7(*a*) and $V/U_m \gtrsim 1$ in figure 7(*b*), and small R/δ cases ($R/\delta = 3$–4).

5. Turbulence in the wall shear stress

As seen from figures 2 and 4, turbulence generated by the oscillatory-flow-alone and combined-flow processes must be a function of the phase, ωt. For instance, figure 8(*b*) illustrates how the r.m.s. value of the fluctuating wall shear stress, $(\widetilde{\tau_0'^2})^{1/2}$, varies over the cycle of the oscillatory motion in the case where the combined flow has the following combination of Reynolds numbers: $Re_c = 2.7\times10^4$, and $Re_w = 2.4\times10^5$ for the 19 cm diameter pipe ($R/\delta = 53$). Here, τ_0', the fluctuating wall shear stress, is

$$\tau_0' = \tau_0 - \tilde{\tau}_0 \tag{11}$$

in which $\tilde{\tau}_0$ is the ensemble-mean wall shear stress (equation (3)). As seen, $(\widetilde{\tau_0'^2})^{1/2}$ experiences one maximum over the flow cycle (fig. 8*b*). (In the oscillatory-flow-alone case, obviously $(\widetilde{\tau_0'^2})^{1/2}$ experiences two maxima due to symmetry, one for each half-cycle, figure 8*a*.)

Figures 9(*a*) and 9(*b*) display the contour plots of the maximum value of this quantity, $(\widetilde{\tau_0'^2})^{1/2}_{max}$, normalized by the maximum value of the mean wall shear stress τ_{max} (see figure 8*b*). In the case of the oscillatory-flow alone, τ_{max} is replaced by τ_w (figure 8*a*), and in the case of the steady current, τ_{max} is replaced by τ_c, the mean wall shear stress.

First, figure 9 shows that there are three distinct flow regimes:

(i) The laminar regime where $(\widetilde{\tau_0'^2})^{1/2}_{max}/\tau_{max} = 0$.

(ii) The transitional regime where $(\widetilde{\tau_0'^2})^{1/2}_{max}/\tau_{max}$ is in the range 0 – 0.25, or 0.35–0.45 (this latter range will be discussed later in the section).

(iii) The fully developed turbulent regime where $(\widetilde{\tau_0'^2})^{1/2}_{max}/\tau_{max} = 0.25$–$0.35$.

Secondly, the data in figure 9 reveal that $(\widetilde{\tau_0'^2})^{1/2}_{max}/\bar{\tau}_0 = 0.25$–$0.34$ when $Re_w = 0$ (the steady-current case) for large Re_c (the fully developed turbulent regime); this is in fairly good agreement with the range, 0.25–0.40, reported in conjunction with the steady-current boundary-layer research (Alfredson *et al.* 1988; Eckelmann 1974; Mitchell & Hanratty 1966, among others).

Thirdly, the data further show that the corresponding interval for the case when $Re_c = 0$ (the oscillatory-flow-alone) for large Re_w (the fully developed turbulent

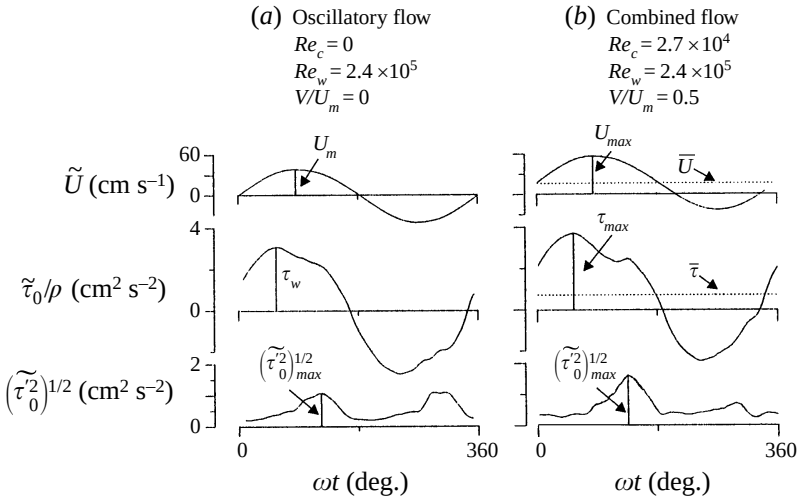

FIGURE 8. Variation of the ensemble-mean of the wall shear stress and the r.m.s. value of the fluctuating wall shear stress with phase over one cycle of the flow. $R/\delta = 53$.

regime) is $(\widetilde{\tau_0'^2})^{1/2}_{max}/\tau_w = 0.25$–$0.30$. This is in good agreement with the previous oscillatory-boundary layer research (Jensen *et al.* 1989).

Fourthly, the figures reveal that the intensity of turbulence in the wall shear stress, $(\widetilde{\tau_0'^2})^{1/2}_{max}/\tau_{max}$, apparently remains practically constant for large values of Re_c and Re_w, at the value of about 0.25–0.35, no matter whether the flow is one of the fundamental flows (the steady current, or the oscillatory flow), or the combined flow.

Finally, the substantial increase in the turbulence intensity in the upper portion of the diagrams in figure 9, namely the area where $0.35 < (\widetilde{\tau_0'^2})^{1/2}_{max}/\tau_{max} < 0.45$, is due to the turbulent spikes experienced in the deceleration stage in the transition-to-turbulence process, just prior to the reversal of the wall shear stress (figures 2 and 4).

6. Mean wall shear stress

The time-averaged mean wall shear stress, $\overline{\tau}$, is defined as the period-averaged value of the ensemble-averaged wall shear stress:

$$\overline{\tau} = \frac{1}{T}\int_0^T \tilde{\tau}_0(\omega t)\,\mathrm{d}t \tag{12}$$

in which $\tilde{\tau}_0(\omega t)$ is the ensemble-mean shear stress (equation (3)). Obviously, $\overline{\tau}$ represents an overall mean (the wall shear stress is first ensemble-averaged, and then period-averaged).

Figures 10(*a*) and 10(*b*) present the data on this quantity normalized by τ_c, namely $\overline{\tau}/\tau_c$, in which τ_c is the mean wall shear stress corresponding to the current component of the combined flow.

The vertical arrows in figure 10 indicate that, at these points, $V/U_m = 1$. The regions to the left of these points correspond to the current-dominated flow regime, and the regions to the right of these points correspond to the wave-dominated flow regime. (Obviously, there must be a range of V/U_m around $V/U_m = 1$ where both components of the flow are equally significant.)

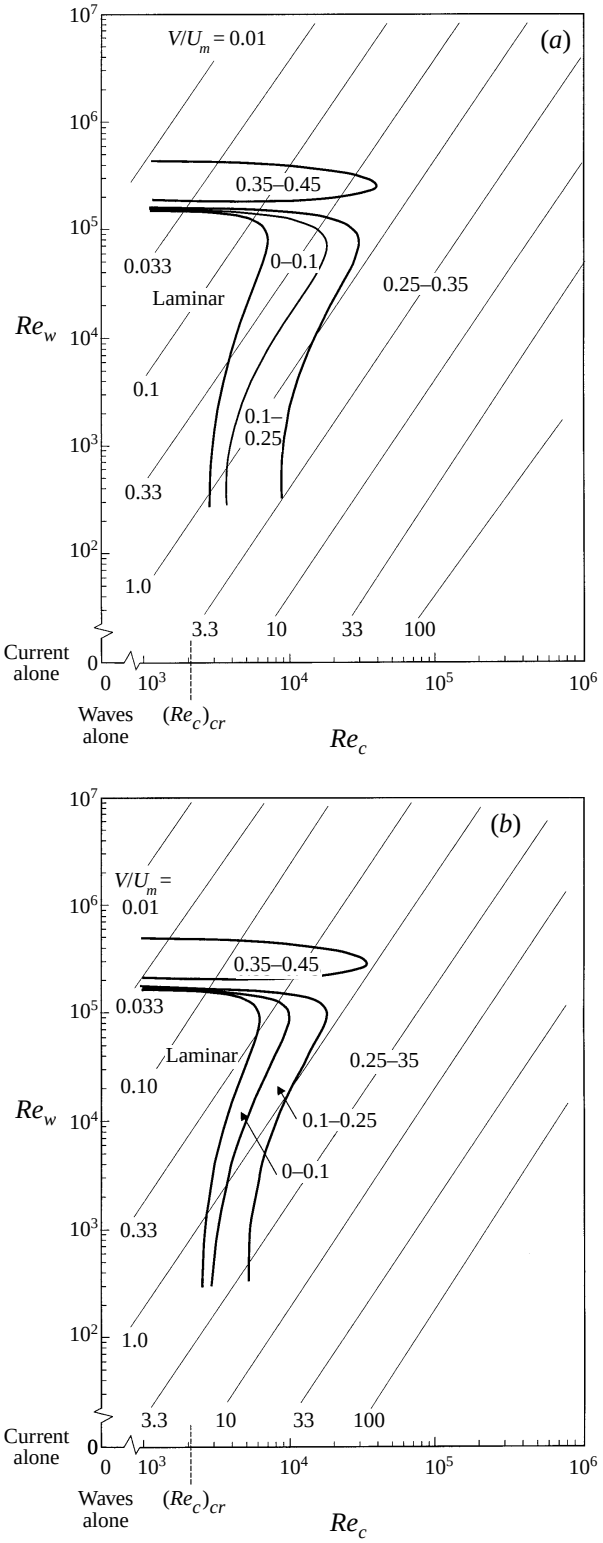

FIGURE 9. Contour plot of $((\widetilde{\tau_0'^2})^{1/2}_{max}/\tau_{max}$ (see figure 8 for the definition): (*a*) $R/\delta = 53$, (*b*) $R/\delta = 25$.

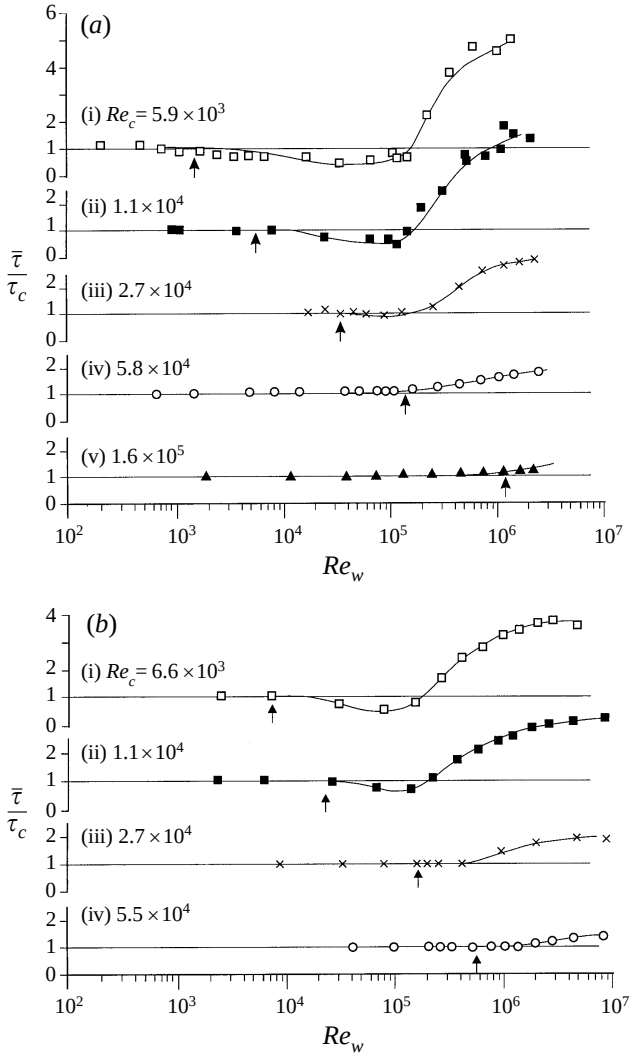

FIGURE 10. Mean wall shear stress normalized by the current wall shear stress. The vertical arrows indicate that, at these points, $V/U_m = 1$. (*a*) $R/\delta = 53$, (*b*) $R/\delta = 25$.

Clearly, the ratio $\bar{\tau}/\tau_c$ will have to be unity if a linear interaction takes place between the current component and the oscillatory-flow component of the combined flow.

Figure 10 shows that:

(i) $\bar{\tau}/\tau_c$ can be unity (no change in the current mean wall shear stress when an oscillatory flow is superimposed).

(ii) It can be smaller than unity (a decrease in the mean wall shear stress with respect to τ_c).

(iii) It can be larger than unity (an increase in the mean wall shear stress with respect to τ_c).

The way in which $\bar{\tau}/\tau_c$ varies with Re_w in figure 10 is shown schematically in figure 11. There are apparently two distinct patterns, figures 11(*a*) and 11(*b*). In the former, $\bar{\tau}/\tau_c$ first decreases, and then increases with increasing Re_w (see figures 10*a*, curves (i), (ii) and to a smaller degree (iii), and also see figure 10*b*, (i) and (ii)), while in the latter

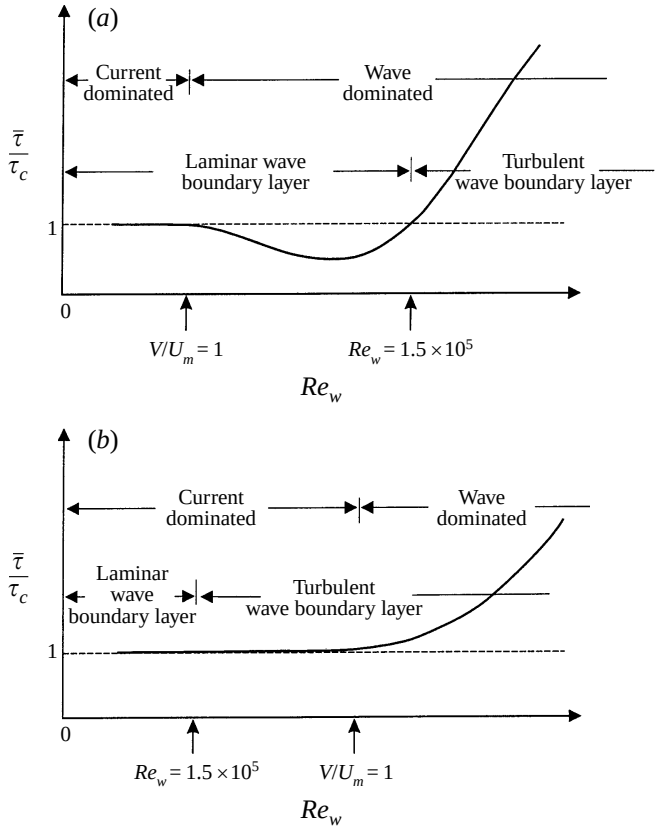

FIGURE 11. Schematic description of the variation of the normalized mean wall shear stress with Re_w for a given Re_c. Two distinct patterns appear: (*a*) and (*b*).

(figure 11*b*), it increases (without experiencing any decrease) with increasing Re_w (figures 10*a* (iv) and (v), and 10*b* (iii) and (iv)).

The decrease in the mean wall shear stress occurs (figures 10(*a*) (i), (ii), (iii) and 10(*b*) (i), (ii)), because the flow becomes wave-dominated, plus the Re_w of the flow is such that the oscillatory boundary layer of the flow is in the laminar regime ($Re_w < 1.5 \times 10^5$) (figure 11*a*); the ranges of Re_w where this decrease is experienced are the ranges where the turbulence is completely (re-laminarization), or heavily suppressed ($0 \leqslant (\overline{\tau_0'^2})^{1/2}_{max}/\tau_{max} \gtrsim 0.1$ (cf. figure 9). This means that the momentum-rich, high-speed flow from the upper portion of the boundary layer is no longer brought into the neighbourhood of the wall by the flow turbulence, because the turbulence is suppressed by the re-laminarization process; the end result is therefore a decrease in the mean wall shear stress. Figure 10 shows that the mean wall shear stress in these regions can easily take values as small as $\bar{\tau}/\tau_c = O(0.5)$, a factor of 2 decrease in $\bar{\tau}$.

By contrast, the mean wall shear stress increases (figure 10) when the flow becomes wave-dominated but the oscillatory boundary layer of the flow is in the turbulent regime ($Re_w > 1.5 \times 10^5$) (figure 11*a*, *b*). This is apparently due to the turbulence generated by the oscillatory boundary layer of the flow. The momentum-rich, high-speed flow (brought into the neighbourhood of the wall by this turbulence) in this case penetrates much closer to the wall owing to the much smaller wave-boundary layer thickness. Hence, the end result will be an increase in the mean wall shear stress.

Lundgren (1972), Grant & Madsen (1979) and Fredsøe (1984) have introduced the concept of 'wave roughness' felt by the current to include this increase in the bed shear stress in modelling of the combined flow.

It is interesting to note that even the fact that the oscillatory boundary layer becomes turbulent is not enough for the mean wall shear stress to be affected, unless the flow becomes wave-dominated (figure 11*b*). (As long as the flow remains current-dominated, no change will occur to the mean wall shear stress).

Figures 12(*a*) and 12(*b*) present the entire data on the (Re_w, Re_c)-plane in the form of contour plots. It may be noted that the increase in the wall shear stress with respect to its steady-current value can be as much as by a factor of 4.

The preceding findings explain qualitatively the results obtained by the previous researchers experimenting with actual wave boundary layers in wave flumes. The existing data have been plotted by R. R. Simons in the paper by Soulsby *et al.* (1993): Kemp & Simons' (1982, 1983) data indicate that while the mean bottom shear stress increase quite substantially in the case of a rough bottom (the transitional/turbulent-regime wave boundary layer), it is not radially different from the current-alone value in the case of a smooth bottom (the laminar-regime wave boundary layer, $Re_w = O(10^3)$). Likewise, Simons *et al.*'s (1988) data indicate a substantial increase in the bottom shear stress; this is because the bottom of the wave flume was covered by gravel in their experiments, and the wave boundary layer was in the transition/turbulent regime.

The friction coefficient for the combined flow, corresponding to the mean wall shear stress, is defined by

$$\bar{f} = 2\frac{\bar{\tau}}{\rho V^2}. \tag{13}$$

Figures 13(*a*) and 13(*b*) depict the present friction-coefficient data plotted against the velocity ratio U_m/U_{fc}, adopting the representation used by Fredsøe (1984). Here, U_{fc} is the friction velocity of the current component of the combined flow:

$$U_{fc} = (\tau_c/\rho)^{1/2}. \tag{14}$$

Figure 13 also includes the values of the friction coefficient found from the Nikuradse diagram (the arrows on the vertical axes) (Schlichting 1979, p. 598) when $U_m/U_{fc} = 0$, the steady-current case. The present values are in reasonable agreement with the Nikuradse values (the discrepancy is within 15–20 % in the worst case).

Figure 13 shows that the friction coefficient varies with U_m/U_{fc} in much the same way as in figure 10. Of particular interest is the dip experienced by the friction coefficient for $Re_c = 5.9\times10^3$, 1.1×10^4, and 2.7×10^4 in figure 13(*a*), and $Re_c = 5.9\times10^3$, and 1.1×10^4 in figure 13(*b*). This corresponds to the fall in $\bar{\tau}/\tau_c$ in figures 11 and 12 where $\bar{\tau}/\tau_c < 1$.

It may be noted that the way in which the friction coefficient changes with U_m/U_{fc} is similar to that obtained theoretically by Fredsøe (1984), using the depth-integrated momentum equation with a logarithmic velocity distribution both inside and outside the wave boundary layer. However, neither in Fredsøe's work nor in more refined flow modelling studies (such as Grant & Madsen's 1979 eddy viscosity model, or Davies *et al.*'s (1988) turbulent-energy closure model), could the previously mentioned dips be captured, because these are related to the wave boundary layer processes where the turbulence is heavily or completely suppressed, as described in the preceding paragraphs.

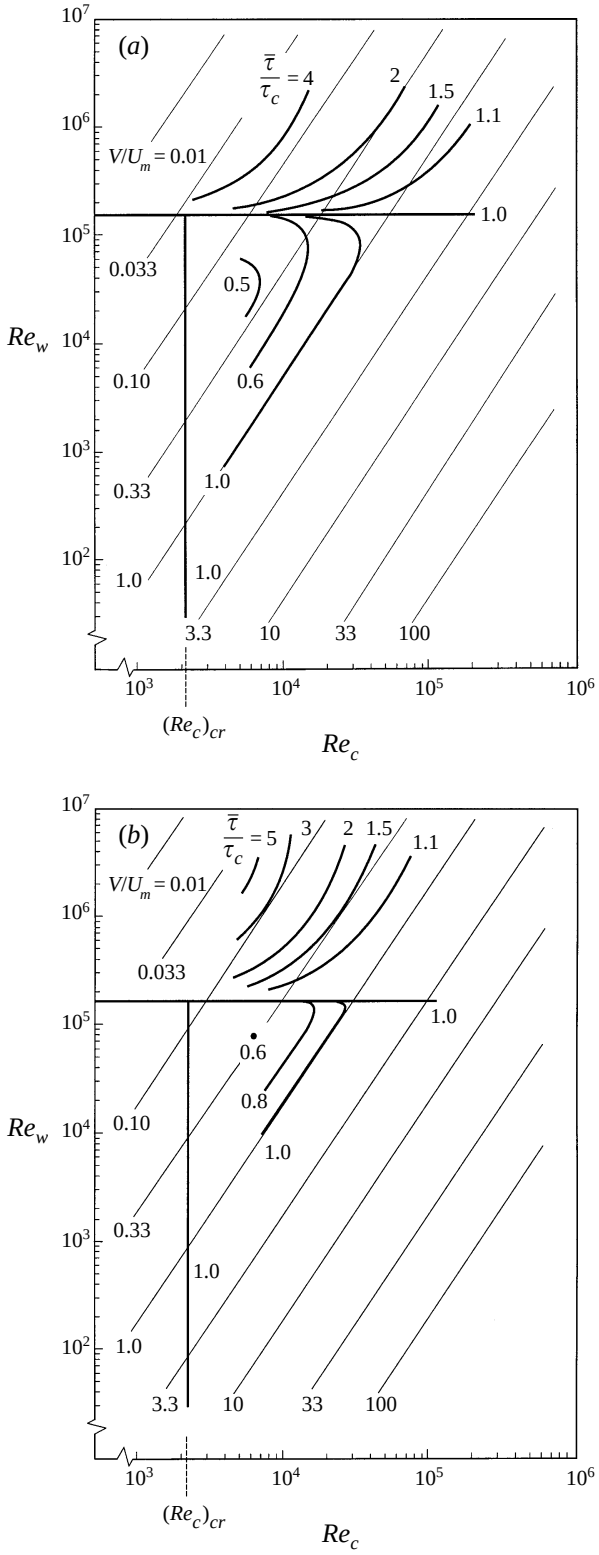

FIGURE 12. Increase in the mean wall shear stress with respect to its steady-current value, based on the same experiments as shown in (*a*) figure 10(*a*) ($R/\delta = 53$) and (*b*) figure 10(*b*) ($R/\delta = 25$).

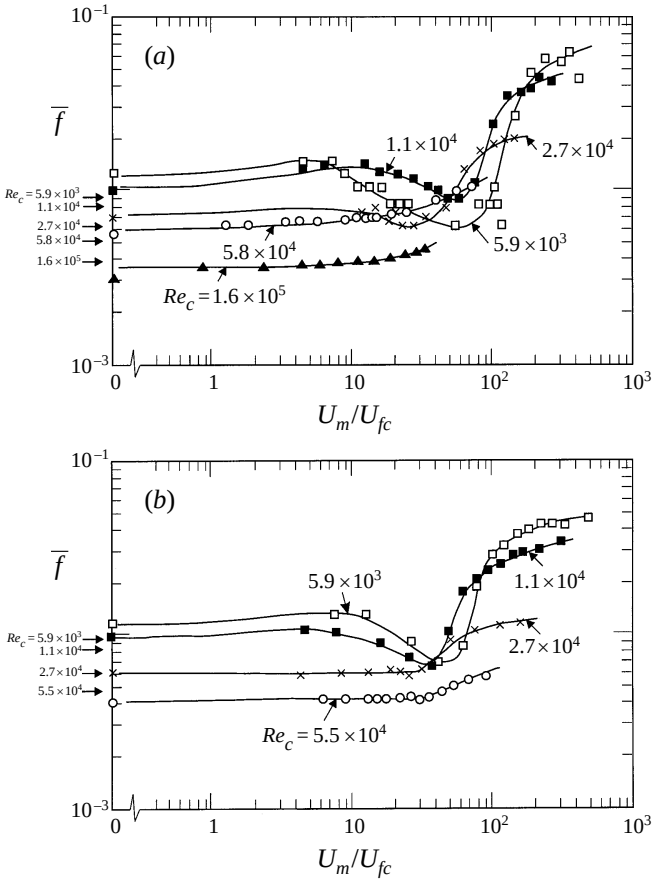

FIGURE 13. Friction coefficient corresponding to the mean wall shear stress (equation (13)). The arrows on the vertical axis indicate the values of the friction coefficient found from the Nikuradse diagram. (*a*) $R/\delta = 53$, (*b*) $R/\delta = 25$.

Finally, figures 14(*a*) and 14(*b*) present the flow-resistance data in terms of the apparent roughness, k_w. Here, k_w is defined by the familiar resistance formula

$$\frac{V}{\overline{U_f}} = 2.46 \ln\left(\frac{7.4R}{k_w}\right) \tag{15}$$

in which k_w is Nikuradse's equivalent sand roughness (Schlichting 1979, p. 621), and represents the roughness caused by the wave boundary layer, and $\overline{U_f}$ is the friction velocity corresponding to the mean wall shear stress, $\overline{U_f} = (\bar{\tau}/\rho)^{1/2}$. For convenience, k_w in figure 14 is normalized by k_s, the roughness obtained from (15) in the case of the steady current (k_w in (15) is replaced by k_s, and $\overline{U_f}$ by U_{fc}). (The actual values of k_s were found in the range $2 \lesssim k_s U_{fc}/\nu \lesssim 8$, which is not radically different from $k_s U_{fc}/\nu \approx 4$, the value corresponding to a smooth wall, Monin & Yaglom 1973, p. 289.)

As seen from figure 14, the wave-induced apparent roughness experiences a variation similar to the friction coefficient (cf. figure 13). The figure further shows that the apparent roughness increases tremendously with increasing U_m/U_{fc} in the wave-dominated, turbulent regime.

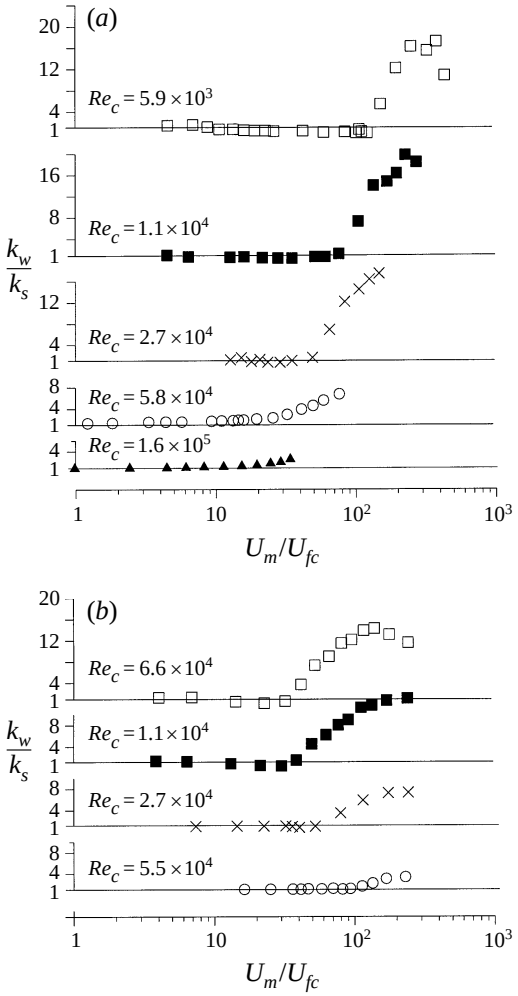

FIGURE 14. Apparent roughness (caused by the oscillatory component of the flow (equation (15)) normalized by the Nikuradse equivalent sand roughness experienced in the case of the steady current alone. (*a*) $R/\delta = 53$, (*b*) $R/\delta = 25$.

7. Oscillating component of the wall shear stress

One of the quantities related to the oscillating component of the wall shear stress is τ_{max}, the maximum value (see figure 8*b* for the definition). Figures 15(*a*) and 15(*b*) display the variation of this quantity normalized by $\tau_c + \tau_w$ in which τ_w is the maximum wall shear stress corresponding to the oscillatory component of the combined flow (figure 8*a*). Obviously, $\tau_{max}/(\tau_c + \tau_w)$ is equal to unity in the case of a linear interaction. Figure 15 indicates that, for the majority of the cases, this interaction is nonlinear. It may be noted that τ_{max} also contains the contribution from the nonlinear interaction for the mean wall shear stress, $\bar{\tau}$, itself (figure 10).

The influence of a superimposed current on the maximum wall shear stress can be described by the quantity $\tau_{max} - \bar{\tau}$, the actual oscillating component of the wall shear stress (figure 8*b*).

In the case of the oscillatory-flow alone (the reference case), $\bar{\tau}$ is zero, and therefore

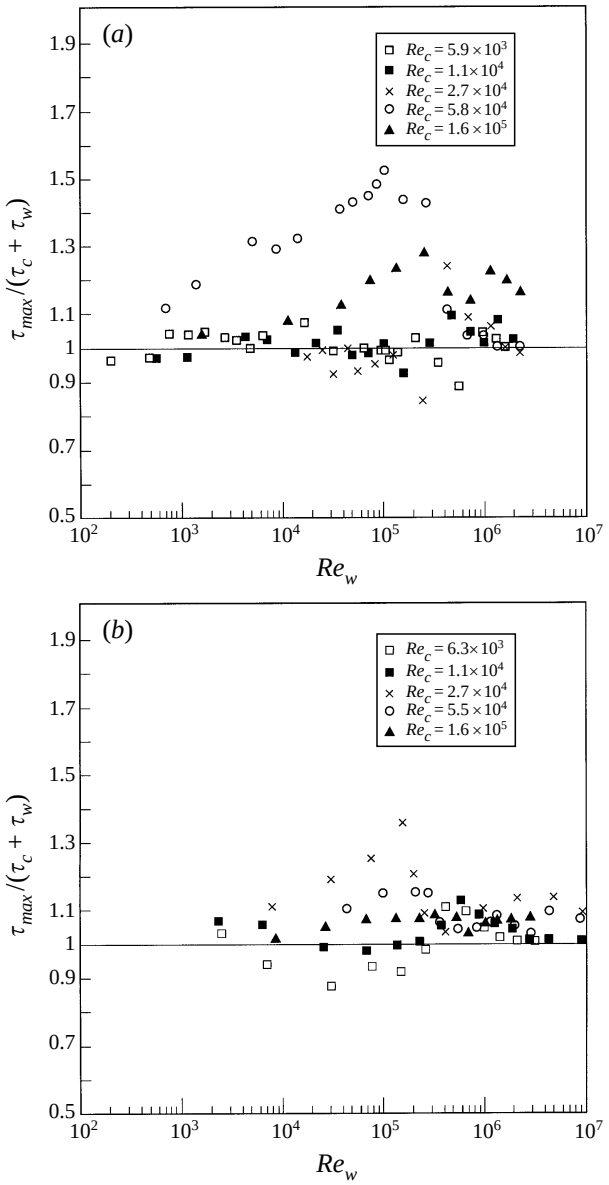

FIGURE 15. Maximum wall shear stress. (*a*) $R/\delta = 53$, (*b*) $R/\delta = 25$.

$\tau_{max} - \bar{\tau} = \tau_w$. Figure 16 presents the data for τ_w in terms of the wave friction coefficient

$$f_w = 2\frac{\tau_w}{\rho U_m^2}. \tag{16}$$

The figure also contains the laminar-flow solution of Uschida (1956) (the straight solid lines).

Figure 16 shows that the laminar friction-coefficient curve for $R/\delta > 7$ branches at $Re_w = 1.5\times10^5$ in the turbulent region where f_w increases with increasing R/δ.

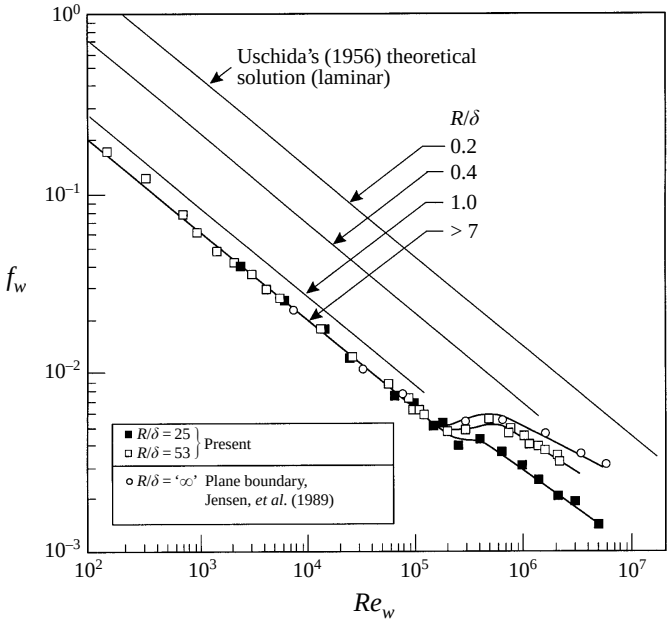

FIGURE 16. Friction coefficient in oscillatory-flow alone (equation (16)).

The data for $\tau_{max}-\bar{\tau}$ in the case of the combined flow are plotted in figures 17(*a*) and 17(*b*) (in the same way as in the previous figure) in which the friction coefficient f_{osc} is defined by

$$f_{osc} = 2\frac{\tau_{max}-\bar{\tau}}{\rho U_m^2}. \tag{17}$$

Clearly, $(\tau_{max}-\bar{\tau})/\tau_w = 1$ or, alternatively, from (16) and (17), $f_{osc} = f_w$, when the interaction is linear. The solid lines in figure 17 represent the linear interaction, namely $f_{osc} = f_w$, taken from figure 16.

Figure 17 indicates the following:

(i) For combinations of small Re_c together with large values of R/δ, the oscillating component of the wall shear stress is practically unaffected by the superposition of a current. The current is felt, however, for large values of Re_c combined with small R/δ, as seen from figure 17(*b*).

(ii) It is interesting to note that the f_{osc} versus Re_w curves in the nonlinear interaction regions appear to be the direct extensions of the turbulent-regime curves into the laminar-flow-regime areas.

The preceding observations suggest that the oscillating part of the combined flow is not affected by the current turbulence for small Re_c (such as $Re_c = 6.6\times10^3$, 1.1×10^4, and 2.7×10^4 when $R/\delta = 53$, and $Re_c = 6.3\times10^3$, and 1.1×10^4 when $R/\delta = 25$), mainly due to the not fully developed turbulent boundary layer (figure 9). However, when the flow becomes a fully developed turbulent boundary layer, the current turbulence begins to influence the oscillating component of the combined flow; no matter what the original regime of the oscillating component of the flow is (laminar, or turbulent), the oscillating boundary layer always becomes turbulent, and hence the momentum-rich, high-speed fluid is brought near the wall by this turbulence, presumably enhancing the oscillatory component of the wall shear stress.

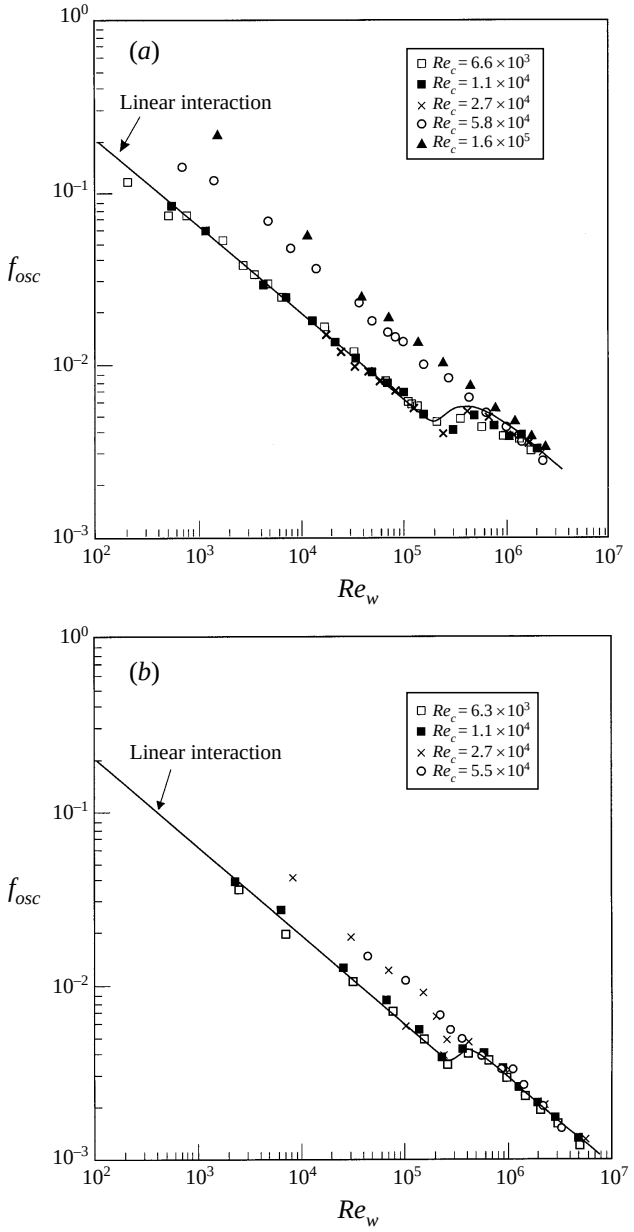

FIGURE 17. Friction coefficient corresponding to the component of the wall shear stress oscillating around the mean wall shear stress (equation (17)). (*a*) $R/\delta = 53$, (*b*) $R/\delta = 25$.

There is comparatively little information on the oscillating component of the bottom shear stress in the case of actual wave boundary layers where the oscillatory flow component is induced by actual waves (Soulsby *et al.* 1993). The laboratory data corresponding to a combined flow where the waves propagate at an angle (at 90°, Sleath 1990, and at 90° and also at values slightly different from 90°, Arnskov *et al.* 1993) suggest that the oscillatory part of the bottom shear stress is close to their corresponding waves-alone values. Likewise, Kemp & Simons' (1982, 1983) experiments (where the waves propagate in the same direction as the current) suggest that

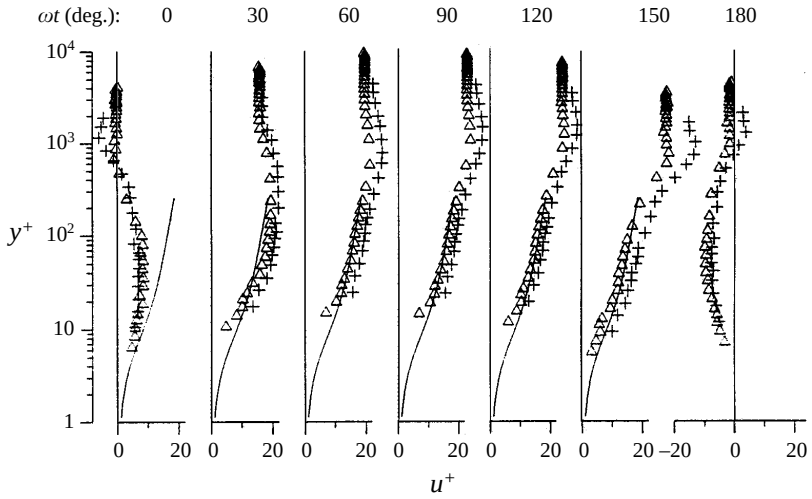

FIGURE 18. Profiles of the ensemble-average velocity at different phase values. Oscillatory-flow alone. $R/\delta = 53$. Triangles: Jensen *et al.* (1989), plane boundary, $Re_w = 1.6 \times 10^6$. Crosses: present experiments, $Re_w = 2.4 \times 10^6$. Solid lines: van Driest profile (equation (18)).

the oscillatory part of the bottom shear stress is practically unaffected by the presence of the current. This may be due to relatively small current Reynolds numbers in these laboratory experiments, as suggested by the present findings.

8. Mean- and fluctuating-velocity profiles

8.1. *Current alone*

The measured velocity profiles $\bar{u}(y)$ (see table 1) were found to compare well with the van Driest profile (van Driest 1956), namely

$$u^+ = 2\int_0^{y^+} \frac{\mathrm{d}y^+}{1+[1+4\kappa^2 y^{+2}(1-\exp(-y^+/A))^2]^{1/2}}, \tag{18}$$

in which u^+ and y^+ are the velocity and the distance from the wall, respectively, normalized by the inner-flow parameters U_{fc} and ν:

$$u^+ = \bar{u}/U_{fc}, \tag{19}$$

$$y^+ = yU_{fc}/\nu, \tag{20}$$

κ is the Kármán constant (≈ 0.4), and A is the van Driest damping factor ($= 25$). The measured turbulence profiles, on the other hand, were found to compare well with the existing data (in Wei & Wilmarth 1989 for $(\overline{u'^2})^{1/2}/U_{fc}$, and in Laufer, 1951, and Durst, Jovanovic & Sender, 1995, for $(\overline{w'^2})^{1/2}/U_{fc}$).

8.2. *Oscillatory-flow alone*

Figure 18 displays the measured velocity profiles in terms of the inner-flow parameters at different phase values for $Re_w = 2.4 \times 10^6$, while figure 19 displays the corresponding

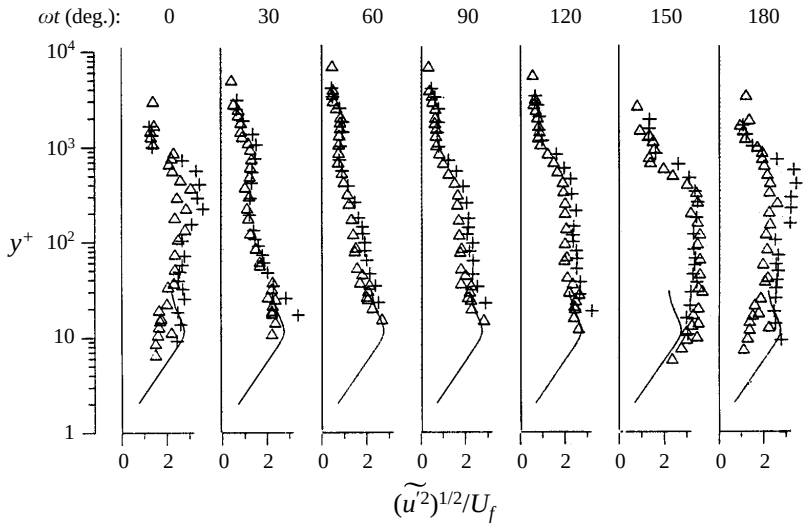

FIGURE 19. Profiles of the r.m.s. value of the fluctuating streamwise velocity at different phase values. Oscillatory-flow alone. $R/\delta = 53$. Symbols as figure 18.

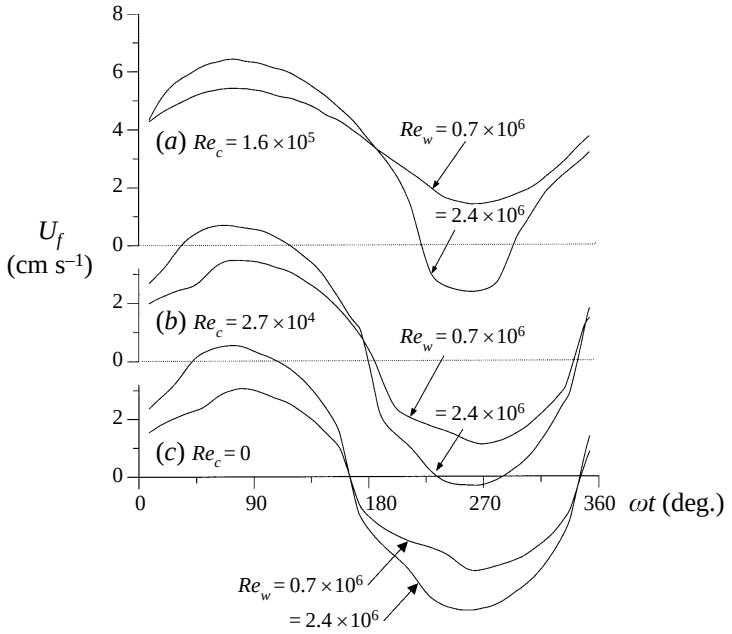

FIGURE 20. Variation of the friction velocity (equation (21)) as a function of phase over one cycle of the flow. $R/\delta = 53$.

turbulence profiles of the r.m.s. values of u'. Here u^+ and y^+ are defined in the same way as in (19) and (20) with $\bar{u}$ replaced by $\tilde{u}(\omega t)$, and U_{fc} replaced by U_f, the friction velocity,

$$U_f(\omega t) = (|\tilde{\tau}_0(\omega t)|/\rho)^{1/2}, \tag{21}$$

corresponding to the given phase value (see figure 20). (The directly measured U_f values, depicted in figure 20, are used in figures 18 and 19.

In figure 18 are plotted the data from the plane-boundary oscillatory-flow research

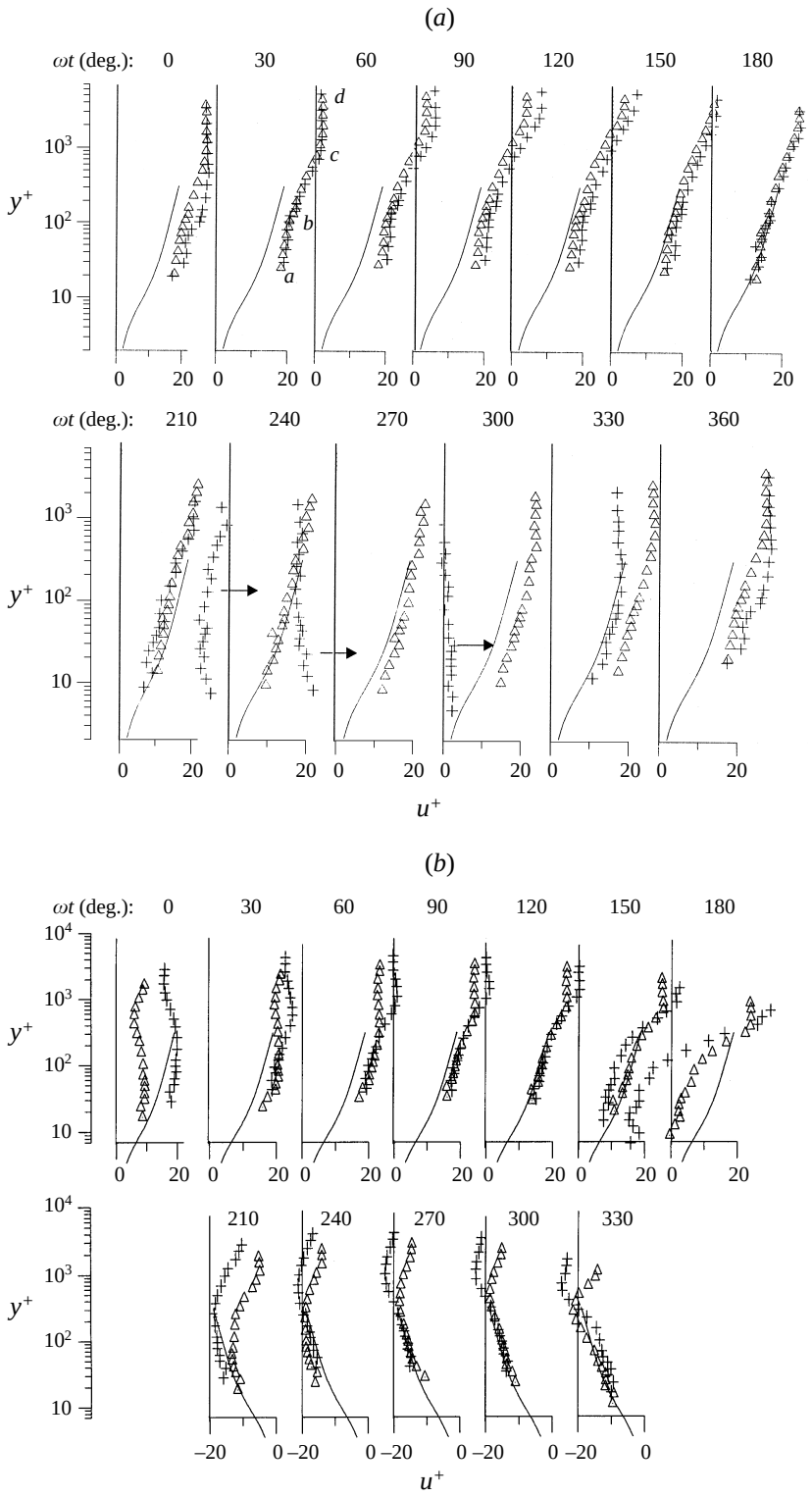

FIGURE 21. (*a*) Profiles of the ensemble-average velocity at different phase values. Combined flow. $R/\delta = 53$. $Re_c = 1.6 \times 10^5$. Triangles: $Re_w = 0.7 \times 10^6$, $V/U_m = 1.3$. Crosses: $Re_w = 2.4 \times 10^6$, $V/U_m = 0.7$. Solid lines: van Driest profile (equation (18)). (*b*) As (*a*) but $Re_c = 2.7 \times 10^4$. Triangles: $Re_w = 0.7 \times 10^6$, $V/U_m = 0.2$. Crosses: $Re_w = 2.4 \times 10^6$, $V/U_m = 0.1$.

also (Jensen *et al.*, 1989), and the van Driest velocity profile (the solid curves) with, again, U_{fc} replaced by U_f (equations (18), (19) and (20)). The phase $\omega t = 0°$ corresponds to the instant when the centreline velocity becomes zero (equation (5)). It appears that the velocity profiles in the present pipe case, and Jensen *et al.*'s plane-boundary case agree quite well. The figure indicates that the logarithmic layer (the straight-line portion of the velocity profile) first emerges around $\omega t = 30°$, and then it gradually grows in size, as the flow progresses. The present profiles are well represented by the van Driest profile with y^+ values up to about 500 for phase values where the pressure gradient ($\partial p/\partial x$) is very small or nil ($\omega t \approx 60°$–$120°$), similar to the case of a steady current (Monin & Yaglom 1973, p. 273).

The turbulence profiles, Jensen *et al.*'s plane boundary data, and the known steady boundary-layer distributions (the solid curves) (see for example, Spalart 1988) are also included in figure 19 for comparison. Here, too, despite some slight differences, the present data and the data from Jensen *et al.*'s study agree quite well. Also, the present data appear to be consistent with the steady-current data, particularly in the phase interval where the pressure gradient is small or nil ($\omega t \approx 30°$–$140°$).

Measurements made for other values of Re_w (0.7 and 6.8×10^6) show similar features.

8.3. *Combined oscillatory flow and current*

Figures 21(*a*) and 21(*b*) show the time development of the velocity profiles, plotted in terms of the inner-flow parameters, over one period of the oscillatory flow in the combined-flow case. As indicated in the figures, the $Re_w = 0.7 \times 10^6$ case in figure 21(*a*) represents a current-dominated case ($V/U_m = 1.3$), while the two cases in figure 21(*b*) represent two wave-dominated cases ($V/U_m = 0.22$ and 0.12). In figure 21, the van Driest velocity profile (the solid lines) is retained in all the panels as a reference line. The phase definition in the figure is the same as that in figure 8(*b*); in the first half-cycle of the oscillatory flow ($\omega t = 0° - 180°$), the steady current and the oscillatory flow are in the same direction, in the second half-cycle ($\omega t = 180°$–$360°$) the opposite. Figure 21(*a*) shows that the measured velocity profiles now have two distinct straight-line portions near the wall (i.e. two 'logarithmic layers'), namely for instance for $\omega t = 30°$, *ab* and *bc* – different from the steady current case, and also from the pure oscillatory-flow case (cf. figure 18 for the latter case). The lower portion, *ab*, of the velocity profile is apparently associated with the wave boundary layer; as seen from figure 21(*a*), it grows in size, and gradually changes its slope, as the wave boundary layer develops over the first half-cycle ($\omega t = 30°$–$180°$). In the next half-cycle, its slope becomes even larger than that of *bc* (see the profile for $Re_w = 0.7 \times 10^6$). (The velocity profile for $Re_w = 2.4 \times 10^6$ in figure 21(*a*) begins to behave differently, starting a little after $\omega t = 210°$ until about $\omega t = 330°$; this is linked with the more pronounced influence of the oscillatory component of the flow where $V/U_m = 0.7$.) Given the fact that the *ab* logarithmic layer is quite far from the normal level (characterized by the van Driest profile), this log layer obviously cannot be explained by a quasi-steady near-wall layer.

By contrast, the velocity profile displayed in figure 21(*b*) have only one straight line portion near the wall (i.e. one logarithmic layer) for both Re_w. This is because both cases in figure 21(*b*) correspond to the wave-dominated regime, as mentioned previously; hence the resulting picture is somewhat similar to figure 18, the oscillatory-flow-alone case. Furthermore, the figure shows that the $Re_w = 2.4 \times 10^6$ profile reverses earlier than the $Re_w = 0.7 \times 10^6$, and obviously this is because of the larger wave component in the case of $Re_w = 2.4 \times 10^6$.

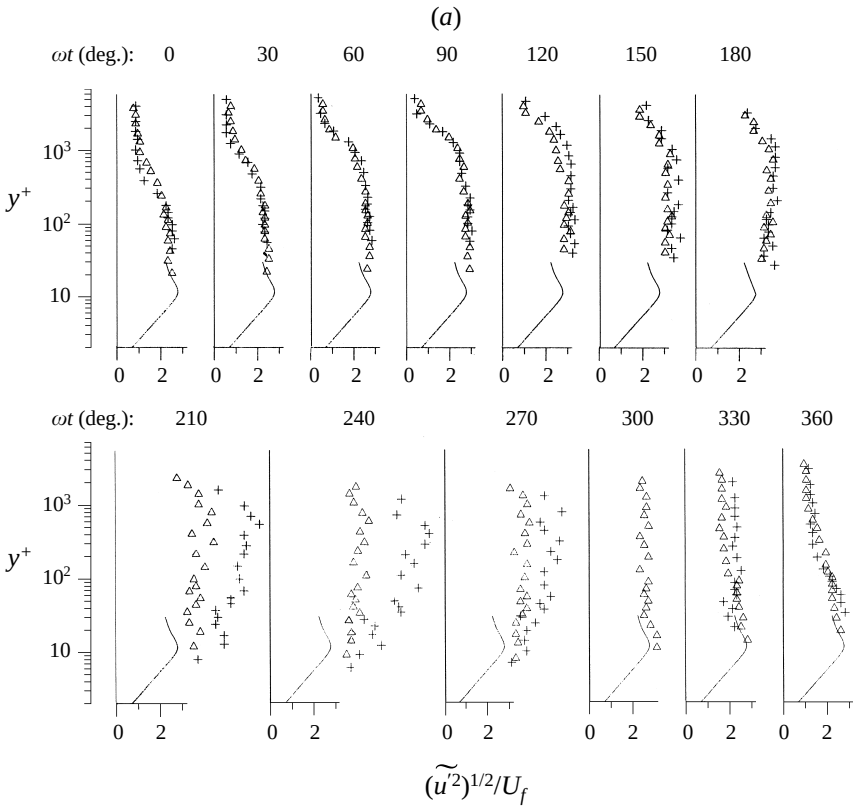

FIGURE 22. For caption see facing page.

Figures 22(*a*) and 22(*b*) illustrate how the $(\widetilde{u'^2})^{1/2}/U_f$ profiles evolve in the phase space. The steady boundary-layer distributions referred to earlier in the previous section are retained in the figures as a reference line (the solid curves).

From figure 22(*a*), it appears that the $(\widetilde{u'^2})^{1/2}/U_f$ profiles are consistent with the steady boundary-layer profiles, except in the phase interval $\omega t = 210°$–$280°$. For these phase values, the magnitude of the combined flow velocity, and hence the wall friction velocity U_f, becomes rather small (figure 20*a*). Therefore, the normalized turbulence quantity $(\widetilde{u'^2})^{1/2}/U_f$ becomes rather large (a factor of 2 larger than the steady boundary-layer values) due to the considerable reduction in the friction velocity.

From figure 22(*b*), it is seen that the turbulence profiles are in remarkable accord with the steady boundary-layer profiles. This is because this flow is a wave-dominated flow, and therefore the resulting picture is expected to be much the same as in figure 19, regardless of the two successive half-periods.

The turbulence data for the tangential velocity component (figure 1) are not given in this paper, but obtainable electronically from the authors at ISVA.

Figure 23 depicts the period-averaged velocity profiles

$$\bar{\tilde{u}}(y) = \frac{1}{T}\int_0^T \tilde{u}(y, \omega t)\,\mathrm{d}t \tag{22}$$

for $Re_c = 1.6 \times 10^5$ for three different cases, namely the current-alone case, and two combined-flows, $Re_w = 2.4 \times 10^6$ and 6.7×10^6. The figure clearly shows that the slope of the straight line portion of the velocity profiles near the wall $(\mathrm{d}\bar{\tilde{u}}/\mathrm{d}y)$ increases when the oscillatory flow is superimposed on the current, meaning that the mean wall shear stress increases with the introduction of the oscillatory flow. From the slope information, while the increase in the mean wall shear stress is $\bar{\tau}/\tau_c = 1.4$ for $Re_w = 2.4 \times 10^6$, it is $\bar{\tau}/\tau_c = 1.7$ for $Re_w = 6.7 \times 10^6$. This is in good agreement with the data obtained from the direct wall shear stress measurements depicted in figure 12(*a*).

Figure 24 presents the period-averaged turbulence velocity profiles

$$\overline{(\widetilde{u'^2})^{1/2}}(y) = \frac{1}{T}\int_0^T (\widetilde{u'^2})^{1/2}(y, \omega t)\,\mathrm{d}t \tag{23}$$

for $Re_c = 1.6 \times 10^5$ for seven different cases, namely the current-alone case, the wave-alone cases $Re_w = 0.7 \times 10^6$, 2.4×10^6 and 6.7×10^6, and their combinations. The current-velocity-to-wave-velocity ratio V/U_m is also indicated in the figure. Figure 24 shows the following features:

(i) From figure 24(*a*) it is seen that the turbulence profile corresponding to the combined flow and that corresponding to the oscillatory flow alone collapse virtually on the same curve, while that corresponding to the current-alone case is totally different.

(ii) By contrast, the turbulence profile corresponding to the combined flow, and that corresponding to the current alone in figure 24(*c*) collapse virtually on the same curve, while that corresponding to the oscillatory-flow-alone case is totally different.

FIGURE 22. Profiles of the r.m.s. value of the fluctuating streamwise velocity at different phase values. Combined flow. $R/\delta = 53$. $Re_c = 1.6 \times 10^5$. Triangles: $Re_w = 0.7 \times 10^6$, $V/U_m = 1.3$. Crosses: $Re_w = 2.4 \times 10^6$, $V/U_m = 0.7$. Solid lines: Steady boundary layer. (Note that the panel corresponding to $\omega t = 300°$ does not contain + symbols, because the friction velocity corresponding to this case at this instant is virtually zero). (*b*) As (*a*) but $Re_c = 2.7 \times 10^4$. Triangles: $Re_w = 0.7 \times 10^6$, $V/U_m = 0.2$. Crosses: $Re_w = 2.4 \times 10^6$, $V/U_m = 0.1$. Solid lines: Steady boundary layer.

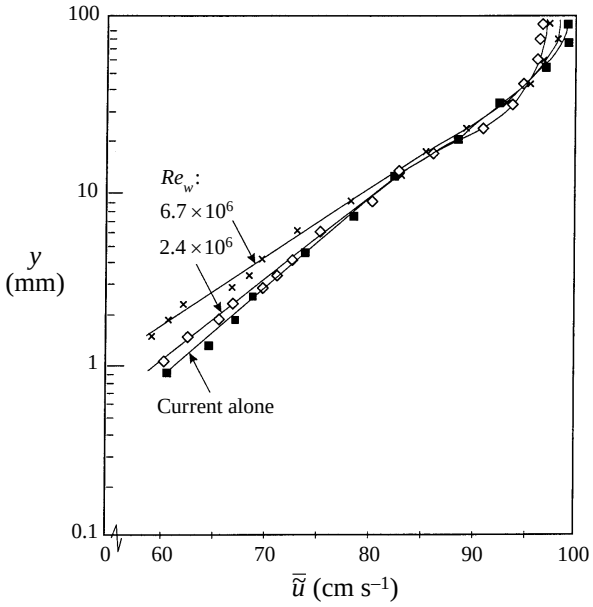

FIGURE 23. Profiles of the period-averaged velocity (equation (22)) for different oscillatory-flow Reynolds number, and $Re_c = 1.6\times10^5$.

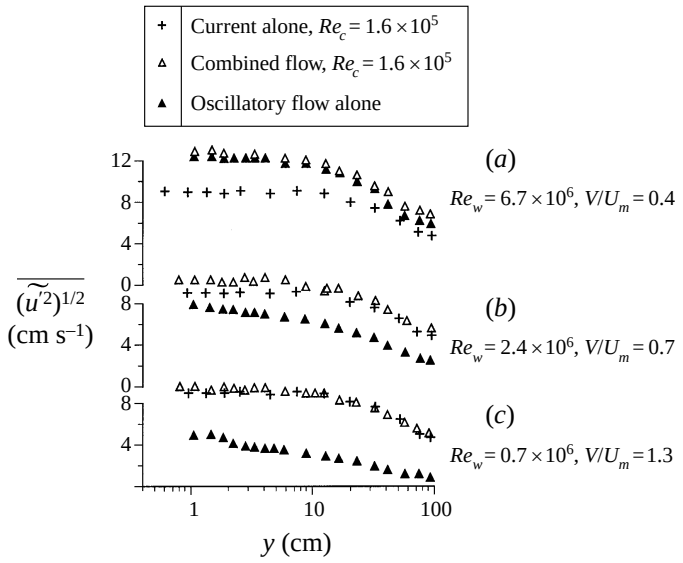

FIGURE 24. Profiles of the period-averaged r.m.s. value of the fluctuating streamwise velocity (equation (23)). $R/\delta = 53$.

This is because, in the former case (figure 24*a*), the combined flow is a wave-dominated flow, and hence the resulting turbulence profile behaves essentially the same as in the case of the oscillatory-flow alone, while, in the latter case (figure 24*c*), the flow is basically a current-dominated flow, and consequently, the turbulence profile behaves much the same as in the case of the current alone. In figure 24(*b*) on the other hand,

the combined-flow turbulence profile near the wall is apparently different from the profiles corresponding to the fundamental cases, basically due to the fact that, in this case, the two components are of equal significance. Also, it may be noted that the turbulence level in the combined flow case is larger (only slightly) than those of the fundamental cases.

The turbulence profiles obtained for the other Re_c where similar measurements were made ($Re_c = 2.7 \times 10^4$) show similar trends.

9. Conclusions

The transition to turbulence in the case of a combined oscillatory flow and current in a pipe is a function of three parameters: the current Reynolds number, Re_c, the oscillatory-flow Reynolds number, Re_w, and the radius-to-Stokes'-layer-thickness, R/δ. The transition to turbulence in the combined-flow case occurs at Re_c larger than the conventional critical value, *ca.* 2×10^3. For instance, for $R/\delta = 53$, and $Re_w = 8 \times 10^4$, the critical value of the Reynolds number is $Re_c = 7 \times 10^3$, a factor of 3.5 increase in the critical value.

A turbulent current can be laminarized by introduction of an oscillatory flow, the re-laminarization. For the re-laminarization of a turbulent current, (*a*) the combined flow needs to be wave dominated, and (*b*) the oscillatory component of the flow needs to be in the laminar flow regime.

When an oscillatory flow is superimposed on a turbulent current, the period-averaged wall shear stress (the mean wall shear stress), $\bar{\tau}$, may retain its value, it may decrease, or it may increase, depending on the flow regime: if the combined flow is in the current-dominated regime ($V/U_m \gtrsim 1$) while the oscillatory-flow component is in the laminar regime ($Re_\omega < 1.5 \times 10^5$), $\bar{\tau}$ retains its current-alone value (linear interaction); if the combined flow is in the wave-dominated regime ($V/U_m \lesssim 1$) while the oscillatory-flow component is in the laminar regime ($Re_w < 1.5 \times 10^5$), $\bar{\tau}$ decreases (nonlinear interaction); if the combined flow is in the wave-dominated regime ($V/U_m \lesssim 1$) while the oscillatory-flow component is in the turbulent regime ($Re_w > 1.5 \times 10^5$), $\bar{\tau}$ increases (nonlinear interaction).

Of particular interest is the increase in the mean wall shear stress. The present results show that this increase can be as much as $O(4$–$5)$ for the test conditions employed in the study, depending on the parameters Re_c, Re_w, R/δ.

The component of the wall shear stress oscillating around $\bar{\tau}$ may retain its oscillatory-flow-alone value, or it may increase, depending on the turbulence level of the combined flow. For an increase, the originally laminar oscillatory boundary layer needs to become a fully developed turbulent boundary layer, when a turbulent current is superimposed. An increase of as much as $O(3$–$4)$ has been measured in the present study for this quantity.

The period-averaged velocity profiles across the cross-section of the pipe near the wall is logarithmic. The period-averaged turbulence profiles across the cross-section of the pipe reveal that: when the flow is in the wave-dominated regime, these profiles are virtually the same as in the oscillatory-flow-alone case; when the flow is in the current-dominated regime, they are essentially the same as in the current-alone case; and otherwise, they are different from those corresponding to the fundamental cases; the turbulence level is generally increased (only slightly) with respect to those in the corresponding fundamental cases.

The data reported in this paper are obtainable in electronic form from the authors at ISVA.

This work has been supported partially by the Danish Technical Research Council (STVF) under the program, Marine Technique, and by the Commission of the European Communities, Directorate General for Science, Research and Development, under MAST contract No. MAS2-CT92-0027, Coastal Morphodynamics, and the final part of the work has been partially supported by MAST contract MAST3-CT97-0081.

REFERENCES

Alfredson, P. H., Johansson, A. V., Haritonidis, J. H. & Eckelmann, H. 1988 The fluctuating wall shear stress and the velocity field in the viscous sublayer. *Phys. Fluids* **31**, 1026–1033.

Arnskov, M. M., Fredsøe, J. & Sumer, B. M. 1993 Bed shear stress over a smooth bed in three-dimensional wave-current flow. *Coastal Engng* **20**, 277–316.

Asano, T., Nakagawa, M. & Iwagaki, Y. 1986 Changes in current properties due to wave superimposing. *Proc. 20th Intl Conf. on Coastal Engng* (ed. B. L. Edge), vol. 1, ch. 70, pp. 925–939. ASCE.

Bakker, W. T. & Doorn, T. van 1978 Near bottom velocities in waves with a current. *Proc. 16th Intl Conf. on Coastal Engng*, *Hamburg* (ed. B. L. Edge), vol. 2, ch. 82, pp. 1394–1413. ASCE.

Bijker, E. W. 1967 Some considerations about scales for coastal models with movable bed. *Publ.* 50. Delft hydraulics Lab., Delft, 142 pp.

Christoffersen, J. B. & Jonsson, I. G. 1985 Bed friction and dissipation in a combined current and wave motion. *Ocean Engng* **12**, 387–423.

Davies, A. G., Soulsby, R. L. & King, H. L. 1988 A numerical model of the combined wave and current bottom boundary layer. *J. Geophys. Res.* **93**, 491–508.

Driest, E. R. van 1956 On turbulent flow near a wall. *J. Aero. Sci.* **23**, 1007–1011.

Durst, F., Jovanovic, J. & Sender, J. 1995 LDA measurements in the near-wall region of a turbulent pipe flow. *J. Fluid Mech.* **295**, 305–335.

Eckelmann, H. 1974 The structure of the viscous sublayer and the adjacent wall region in a turbulent channel flow. *J. Fluid Mech.* **65**, 439–459.

Eckmann, D. M. & Grotberg, J. B. 1991 Experiments on transition to turbulence in oscillatory pipe flow. *J. Fluid Mech.* **222**, 329–350.

Finnicum, D. S. & Hanratty, T. J. 1988 Influence of imposed flow oscillations on turbulence. *Physicochem. Hydrodyn.* **10**, 585–598.

Foster, D. L. 1996 Dynamics of the nearshore wave bottom boundary layer. A Thesis submitted to Oregon State University, in partial fulfillment of the requirements for the degree of doctor of Philosophy.

Foster, D. L., Holman, R. A. & Beach, R. A. 1994 Sediment suspension events and shear instabilities in the bottom boundary layer. *Coastal Dynamics 94*, *Proc. Intl Conf on the Role of the Large Scale Experiments in Coastal Research*, *Universitat Politecnica de Catalunya*, *Barcelona*, *Spain*, *Feb. 21–25*, *1994* (ed. A. S.-Arcilla, M. J. F. Stive & N. C. Kraus), pp. 712–726. ASCE.

Fredsøe, J. 1984 Turbulent boundary layer in wave-current motion. *J. Hydraul. Engng ASCE*, **110**, 1103–1120.

Gilbrech, D. A. & Combs, G. D. 1963 Critical Reynolds numbers for incompressible pulsating flows in tubes. *Developments in Theoretical and Applied Mechanics*, vol. 1, pp. 292–304. Plenum.

Grant, W. D. & Madsen, O. S. 1979 Combined wave and current interaction with a rough bottom. *J. Geophys. Res.* **84**, 1797–1808.

Grant, W. D., Williams, A. J., Glenn, S. M., Cacchione, D. A. & Drake, D. E. 1983 High frequency bottom stress variability and its prediction in the CODE region. *WHOI Tech. Rep.* 83–19. Woods Hole Oceanographic Institute.

Hanratty, T. J. & Campbell, J. A. 1983 Measurement of wall shear stress. In *Fluid Mechanics Measurements* (ed. R. J. Goldstein) pp. 559–615. Hemisphere.

Hino, M., Sawamoto, M. & Takasu, S. 1976 Experiments on transition to turbulence in an oscillatory pipe flow. *J. Fluid Mech.* **75**, 193–207.

HUNTLEY, D. A. & HAZEN, D. G. 1988 Seabed stresses in combined wave and steady flow conditions on the Nova Scotia continental shelf – field measurements and predictions. *J. Phys. Oceanogr.* **18**, 347–362.

HUYNH-THANH, S. & TEMPERVILLE, A. 1991 A numerical model of the rough turbulent boundary layer in combined wave and current interaction. In *Sand Transport in Rivers, Estuaries and the Sea* (ed. R. L. Soulsby & R. Bettess), pp. 93–100. Balkema.

JENSEN, B. L., SUMER, B. M. & FREDSØE, J. 1989 Turbulent oscillatory boundary layers at high Reynolds numbers. *J. Fluid Mech.* **206**, 265–297.

JUSTESEN, P. 1988 Turbulent wave boundary layers. *Series Paper* 41. Inst. Hydrodynamics and Hydraulic Eng., Technical University of Denmark.

KEMP, P. H. & SIMONS, R. R. 1982 The interaction between waves and a turbulent current: waves propagating with the current. *J. Fluid Mech.* **116**, 227–250.

KEMP, P. H. & SIMONS, R. R. 1983 The interaction between waves and a turbulent current: waves propagating against the current. *J. Fluid Mech.* **130**, 73–89.

KESTEREN, W. G. M. VAN & BAKKER, W. T. 1984 Near bottom velocities in waves with a current; analytical and numerical computations. In *Proc. 19th Conf. Coastal Engng, Houston, TX*, pp. 1161–1177. ASCE.

LAUFER, J. 1951 Investigation of turbulent flow in two dimensional channel. *NACA Rep.* 1053.

LUNDGREN, H. 1972 Turbulent currents in the presence of waves. *Proc. 13th Coastal Engng Conf. July 10–14, 1972, Vancouver, B.C.*, Canada, vol. 1, chap. 33. ASCE.

MAO, Z. & HANRATTY, T. J. 1986 Studies of the wall shear stress in a turbulent pulsating pipe flow. *J. Fluid Mech.* **170**, 545–564.

MAO, Z. & HANRATTY, T. J. 1994 Influence of large-amplitude oscillations on turbulent drag. *AIChE J.* **40**, 1601–1610.

MITCHELL, J. E. & HANRATTY, T. J. 1966 A study of turbulence at a wall using an electrochemical wall shear-stress meter. *J. Fluid Mech.* **26**, 199–221.

MONIN, A. S. & YAGLOM, A. M. 1973 *Statistical Fluid Mechanics: Mechanics of Turbulence*. MIT Press.

MYRHAUG, D., REED, K. & FYFE, A. J. 1987 Seabed boundary layer studies for pipelines: Large scale laboratory experiments. In *Proc. 9th Intl Symp. on Offshore Engineering, Rio de Janeiro* (ed. F. L. L. Carneiro *et al.*), pp. 345–359. Wiley.

MYRHAUG, D. & SLAATTELID, O. H. 1989 Combined wave and current boundary layer model for fixed rough seabeds. *Ocean Engng* **16**, 119–142.

MYRHAUG, D. & SLAATTELID, O. H. 1990 A rational approach to wave-current friction coefficients for rough, smooth and transitional turbulent flow. *Coastal Engng*, **14**, 265–293.

RAMAPRIAN, B. R. & TU, S. W. 1980 An experimental study of oscillatory pipe flow at transitional Reynolds number. *J. Fluid Mech.* **100**, 513–544.

RAMAPRIAN, B. R. & TU, S. W. 1983 Fully developed periodic turbulent pipe flow. Part 2. The detailed structure of the flow. *J. Fluid Mech.* **137**, 59–81.

SARPKAYA, T. 1966 Experimental determination of the critical Reynolds-number for pulsating Pouseuille flow. *Trans. ASME: J. Basic Engng*, Sept., 589–598.

SCHLICHTING, H. 1979 *Boundary-Layer Theory*. McGraw-Hill.

SERGEEV, S. I. 1966 Fluid oscillations in pipes at moderate Reynolds numbers. *Mekh. Zhid. i Gaza* **1**, no. 1, 21.

SHEMER, L., WYGNANSKI, I. & KIT, E. 1985 Pulsating flow in a pipe. *J. Fluid Mech.* **153**, 313–337.

SIMONS, R. R., GRASS, T. J. & MANSOUR-TEHRANI, M. 1992 Bottom shear stresses in the boundary layer under waves and currents crossing at right angles. In *Proc. 23rd Intl Conf. on Coastal Engng, Venice, Italy* (ed. B. L. Edge), Vol. 1, Ch. 45, pp. 604–617. ASCE.

SIMONS, R. R., GRASS, T. J., SALEH, W. M. & TEHRANI, M. M. 1994 Bottom shear stresses under waves with a current superimposed. *Proc. 24th Intl Conf. on Coastal Engng, Oct. 1994, Kobe, Japan* (ed. B. L. Edge), vol. 1, ch. 42, pp. 565–578.

SIMONS, R. R., KYRIACOU, A., SOULSBY, R. L. & DAVIES, A. G. 1988 Predicting the nearbed turbulent flow in waves and currents. In Proc. *IAHR Symposium on Mathematical Modelling of Sediment Transport in the Coastal Zone, Copenhagen*, pp. 33–47.

SLEATH, J. F. A. 1990 Velocities and bed friction in combined flow. In *22nd Intl Conf. on Coastal Engineering, Delft, 1990*, vol. 1, pp. 450–463. ASCE.

Sleath, J. F. A. 1991 Velocities and shear-stresses in wave-current flows. *J. Geophys. Res.* **96**, 15237–15244.

Soulsby, R. L., Hamm, L., Klopman, G., Myrhaug, D., Simons, R. R. & Thomas, G. P. 1993 Wave-current interaction in the vertical. *Coastal Engng* **21**, 41–69.

Soulsby, R. L. & Humphery, J. D. 1990 Field observations of wave-current interaction at the seabed. In *Water Wave Kinematics* (ed. A. Tørum & O. T. Gudmester), pp. 413–428. Kluwer.

Spalart, P. R. 1988 Direct simulation of a turbulent boundary layer. *J. Fluid Mech.* **187**, 61–98.

Stettler, J. C. & Hussain, A. K. M. F. 1986 On transition of the pulsatile flow. *J. Fluid Mech.* **170**, 169–197.

Sumer, B. M., Arnskov, M. M., Christiansen, N. & Jørgensen, F. E. 1993 Two-component hot-film probe for measurements of wall shear stress. *Exp. Fluids* **15**, 380–384.

Tardu, S. F., Binder, G. & Blackwelder, R. F. 1994 Turbulent channel flow with large-amplitude velocity oscillations. *J. Fluid Mech.* **267**, 109–151.

Tromans, P. S. 1978 Stability and transition of periodic pipe flows. PhD thesis, Cambridge University.

Tu, S. W. & Ramaprian, B. R. 1983 Fully developed periodic turbulent pipe flow. Part 1. Main experimental results and comparison with predictions. *J. Fluid Mech.* **137**, 31–58.

Uschida, S. 1956 The pulsating viscous flow superposed on the steady laminar motion of incompressible fluid in a circular pipe. *Z. Angew. Math. Phys.* **7**, 403.

Wei, T. & Willmarth, W. W. 1989 Reynolds-number effects on the structure of a turbulent channel flow. *J. Fluid Mech.* **204**, 57–95.